

# Practical block encodings of matrix polynomials that can also be trivially controlled

Martina Nibbi<sup>1, 2, \*</sup> Filippo Della Chiara<sup>1, 3, †</sup> Yizhi Shen<sup>4, ‡</sup> Aaron Szasz<sup>5, §</sup> and Roel Van Beeumen<sup>3, 4, ¶</sup>

<sup>1</sup>These authors contributed equally to this work.

<sup>2</sup>Technical University of Munich, School of Computation,

Information and Technology, Boltzmannstraße 3, 85748 Garching, Germany

<sup>3</sup>Department of Computer Science, KU Leuven, University of Leuven, 3001 Leuven, Belgium

<sup>4</sup>Applied Mathematics and Computational Research Division,

Lawrence Berkeley National Laboratory, Berkeley, CA 94720, USA

<sup>5</sup>Google Quantum AI, Santa Barbara, CA 93111, USA

(Dated: January 27, 2026)

Quantum circuits naturally implement unitary operations on input quantum states. However, non-unitary operations can also be implemented through “block encodings”, where additional ancilla qubits are introduced and later measured. While block encoding has a number of well-established theoretical applications, its practical implementation has been prohibitively expensive for current quantum hardware. In this paper, we present practical and explicit block encoding circuits implementing matrix polynomial transformations of a target matrix. With standard approaches, block-encoding a degree- $d$  matrix polynomial requires a circuit depth scaling as  $d$  times the depth for block-encoding the original matrix alone. By leveraging the recently introduced Fast One-Qubit Controlled Select LCU (FOQCS-LCU) framework, we show that the additional circuit-depth overhead required for encoding matrix polynomials can be reduced to scale linearly in  $d$  with no dependence on system size or the cost of block encoding the original matrix. Moreover, we demonstrate that the FOQCS-LCU circuits and their associated matrix polynomial transformations can be controlled with negligible overhead, enabling efficient applications such as Hadamard tests. Finally, we provide explicit circuits for representative spin models, together with detailed non-asymptotic gate counts and circuit depths.

## I. INTRODUCTION

Quantum circuits act unitarily on input states, but important applications of quantum computing to linear algebra and quantum simulation also require non-unitary operations. These operations can be implemented through block encodings [1–27]. Given a matrix  $\mathcal{H}$ , a block encoding embeds  $\mathcal{H}$  as a sub-block of a larger unitary acting on an extended Hilbert space. This construction enables the implementation of  $\mathcal{H}$  using unitary quantum circuits, with post-selection on ancilla qubits restricting to the desired non-unitary matrix block.

Although well understood theoretically, block encoding has been viewed as impractical on present-day quantum hardware, as the standard routines require large multi-controlled gates and circuits that are non-local on two-dimensional qubit chip architectures. The recently introduced Fast One-Qubit Controlled Select Linear Combination of Unitaries (FOQCS-LCU) framework [27] overcomes the gate-complexity bottleneck for a wide class of matrices  $\mathcal{H}$ , replacing multi-controlled gates with just two parallel layers of two-qubit gates. In exchange, we must use a number of ancilla qubits that scales linearly with the system size. For many important Hamiltonians,

such as one-dimensional Ising and Heisenberg models, the FOQCS-LCU block-encoding yields a short circuit depth that is linear in the number of spins.

Even with the barriers to block encoding removed for large classes of non-unitary matrices, there are further challenges to the practical application of block encodings in useful algorithms. The first key challenge is the controlled application of a block-encoded non-unitary operation. Such controlled block encodings are required, for example, in Hadamard-test circuits. The problem is that, even if a block encoding for  $\mathcal{H}$  can be efficiently decomposed into native one- and two-qubit gates, once the encoding is controlled, we would naively end up with a large number of Toffoli gates. Such circuits would again be impractical on present-day devices. In this paper, we show that FOQCS-LCU block-encodings for a large class of non-unitaries  $\mathcal{H}$  can be controlled with negligible overhead, requiring just two additional CNOT gates compared with the cost of the non-controlled block encoding of  $\mathcal{H}$ .

The second key challenge is the need to block-encode not just  $\mathcal{H}$ , but polynomials of  $\mathcal{H}$ . This arises, for example, in using block encoding to implement time evolution under a quantum spin Hamiltonian, where we approximate the time-evolution operator  $\exp(-i\mathcal{H}t)$  with a suitable polynomial expansion in  $\mathcal{H}$  [12, 28–31]. For common techniques such as the Quantum Singular Value Transformation (QSVT) [13, 29, 30, 32–36], the circuit depth to block-encode a degree- $d$  polynomial in  $\mathcal{H}$  would scale as  $d$  times the depth to encode  $\mathcal{H}$ . In this paper, we generalize the FOQCS-LCU framework and show that the extra circuit depth when encoding a polynomial in  $\mathcal{H}$  relative

\* [martina.nibbi@tum.de](mailto:martina.nibbi@tum.de)

† [filippo.dellachiara@kuleuven.be](mailto:filippo.dellachiara@kuleuven.be)

‡ [yizhis@lbl.gov](mailto:yizhis@lbl.gov)

§ [aszasz@google.com](mailto:aszasz@google.com)

¶ [rvanbeeumen@lbl.gov](mailto:rvanbeeumen@lbl.gov)

to encoding just  $\mathcal{H}$  scales only with  $d$ ; that is, the extra depth for the polynomial is independent of the complexity of the original block encoding of  $\mathcal{H}$  and therefore also independent of system size. Even more striking, the entire block-encoding for the polynomial can additionally be controlled by adding just 4 CNOT gates, independent of system size and of the polynomial degree.

Furthermore, we show that our block encodings can be efficiently implemented on quantum chips with realistic two-dimensional layouts using only local (nearest-neighbor and single-qubit) gates. We first provide explicit circuit constructions in terms of single- and two-qubit gates assuming all-to-all connectivity, from which we derive exact, non-asymptotic CNOT gate counts and circuit depths. We then provide a detailed mapping of those circuits to a two-dimensional square grid architecture, with the final circuit written only in terms of local gates in 2D: single-qubit gates and nearest-neighbor two-qubit gates. The mapping from all-to-all to 2D incurs only a small overhead—the increase in circuit depth is just a few layers, independent of the system size.

To summarize, for important classes of non-unitary operators  $\mathcal{H}$ , including 1D quantum spin models, this paper resolves many of the bottlenecks that have made block encoding impractical until now:

- (1) The block encoding of  $\mathcal{H}$  can be controlled with negligible overhead.
- (2) Block encodings of matrix polynomials in  $\mathcal{H}$  are nearly as efficient as block-encodings of  $\mathcal{H}$  alone.
- (3) Block encodings of matrix polynomials in  $\mathcal{H}$  can be controlled with negligible overhead.
- (4) All of these block encodings can be implemented in low-depth circuits using only nearest-neighbor two-qubit gates on a two-dimensional square lattice.

By introducing explicit and practical circuits, our framework turns block encodings and controlled block encodings from theoretical abstractions into concrete modules that can be compiled, benchmarked, and stress-tested.

**Road map.** The paper is organized as follows. Section II discusses the simplification of a generic controlled multi-qubit gate when it acts on special reference states. This is a key ingredient for our main results on controlled block encodings. In Section III, we examine block encodings via the FOQCS-LCU formalism, originally conceptualized in [27], and further develop the construction and implementation of its controlled versions. In Section IV, we proceed to show how to realize a matrix polynomial in a generic operator  $\mathcal{H}$  given its FOQCS-LCU block encoding and discuss how to implement a controlled version of the polynomial matrix transformations with negligible overhead. In Section V, we outline explicit circuits and potential applications of FOQCS-LCU-enabled block encodings of matrix polynomials, in both uncontrolled and controlled forms. We conclude and summarize in Section VI.

## II. CONTROLLED UNITARIES AND COMMON EIGENSTATES

Controlled unitaries are essential and ubiquitous building blocks in many quantum algorithms. In this section, we consider unitaries with a decomposition of the form

$$\mathcal{U} = B_s \cdot A_s \cdots B_1 \cdot A_1, \quad (1)$$

where we assume that the unitaries  $\{A_i\}_{i=1}^s$  can be implemented using very few elementary gates, and the unitaries  $\{B_i\}_{i=1}^s$  share a common eigenstate  $|\xi\rangle$  corresponding to eigenvalue 1:

$$B_i |\xi\rangle = |\xi\rangle, \quad \forall i = 1, \dots, s. \quad (2)$$

Next we prove that a controlled version of such unitaries  $\mathcal{U}$ , whenever *applied to* or *measured in* the state  $|\xi\rangle$ , can be efficiently implemented with only negligible overhead compared to the implementation of  $\mathcal{U}$  itself.

### A. Applying controlled unitaries to a specific state

Controlling a unitary of the form Eq. (1) leads to the following lemma, which formalizes how such controlled implementations can be efficiently realized when applied to the specific common eigenstate  $|\xi\rangle$ .

**Lemma 1.** *Let  $\mathcal{U}$  be defined as in Eqs. (1) and (2), with  $|\xi\rangle$  a common eigenstate of  $\{B_i\}_{i=1}^s$ . Then, the controlled application of  $\mathcal{U}$  to  $|\xi\rangle$  can be simplified as follows:*

$$|\xi\rangle \xrightarrow{n} \mathcal{U} = |\xi\rangle \xrightarrow{n} A_1 \cdot B_1 \cdot \cdots \cdot A_s \cdot B_s \quad (3)$$

*Proof.* Let the control qubit be prepared in an arbitrary superposition  $\alpha|0\rangle + \beta|1\rangle$ . Then the left-hand side of Eq. (3) yields the following joint state:

$$(\alpha|0\rangle + \beta|1\rangle)|\xi\rangle \longrightarrow \alpha|0\rangle|\xi\rangle + \beta|1\rangle\mathcal{U}|\xi\rangle, \quad (4)$$

while the right-hand side yields the state:

$$\begin{aligned} (\alpha|0\rangle + \beta|1\rangle)|\xi\rangle &\longrightarrow \\ \alpha|0\rangle \prod_{i=1}^s B_i |\xi\rangle + \beta|1\rangle \prod_{i=1}^s B_i A_i |\xi\rangle. \end{aligned} \quad (5)$$

Next, using the eigenstate properties in Eq. (2) and the decomposition in Eq. (1), we obtain:

$$\alpha|0\rangle \prod_{i=1}^s B_i |\xi\rangle = \alpha|0\rangle|\xi\rangle, \quad (6)$$

$$\beta|1\rangle \prod_{i=1}^s B_i A_i |\xi\rangle = \beta|1\rangle\mathcal{U}|\xi\rangle. \quad (7)$$

Inserting Eqs. (6) and (7) into Eq. (5) yields Eq. (4), completing the proof.  $\square$

As a consequence, it suffices to only control the unitaries  $A_i$ . Under the assumption that the implementation costs of  $A_i$  are negligible relative to those of  $B_i$ , the controlled unitary acting on  $|\xi\rangle$  has a cost comparable to its non-controlled implementation.

## B. Measuring controlled unitaries in a specific state

From Lemma 1, we can derive similar simplifications for the measurement of a controlled unitary. These are summarized in the following lemma and corollary, where  $P_\xi$  is defined to be a unitary that prepares the common eigenstate of  $\{B_i\}_{i=1}^s, |\xi\rangle$ :

$$|\xi\rangle = P_\xi |0\rangle_n. \quad (8)$$

**Lemma 2.** *Let  $\mathcal{U}$  be defined as in Eqs. (1), (2) and (8). Then, the controlled application of  $\mathcal{U}$  to an arbitrary  $n$ -qubit state  $|\varphi\rangle$ , followed by a measurement post-selected on the outcome  $|\xi\rangle$ , can be simplified as follows:*

$$\begin{aligned} |\varphi\rangle \not\perp^n \mathcal{U} \not\perp P_\xi^\dagger \not\perp 0 &= \\ |\varphi\rangle \not\perp^n A_1 \not\perp B_1 \not\perp \dots \not\perp A_s \not\perp B_s \not\perp P_\xi^\dagger \not\perp 0 &= \end{aligned} \quad (9)$$

*Proof.* Starting from a generic control-qubit state  $\alpha|0\rangle + \beta|1\rangle$ , the left-hand side of Eq. (9) produces the following joint state before the measurement:

$$(\alpha|0\rangle + \beta|1\rangle)|\varphi\rangle \longrightarrow \alpha|0\rangle P_\xi^\dagger |\varphi\rangle + \beta|1\rangle P_\xi^\dagger \mathcal{U} |\varphi\rangle. \quad (10)$$

Consequently, when the bottom  $n$  qubits are measured in the state  $|0\rangle$ , we obtain:

$$\alpha|0\rangle \langle \xi | \varphi \rangle + \beta|1\rangle \langle \xi | \mathcal{U} |\varphi\rangle. \quad (11)$$

On the other hand, the right-hand side of Eq. (9) produces, before measurement, the joint state:

$$\begin{aligned} (\alpha|0\rangle + \beta|1\rangle)|\varphi\rangle \longrightarrow \\ \alpha|0\rangle P_\xi^\dagger \prod_{i=1}^s B_i |\varphi\rangle + \beta|1\rangle P_\xi^\dagger \prod_{i=1}^s B_i A_i |\varphi\rangle, \end{aligned} \quad (12)$$

and after measuring the bottom  $n$  qubits in the state  $|0\rangle$ , we obtain:

$$\alpha|0\rangle \langle \xi | \prod_{i=1}^s B_i |\varphi\rangle + \beta|1\rangle \langle \xi | \prod_{i=1}^s B_i A_i |\varphi\rangle. \quad (13)$$

Next, we note that, as  $B_i$  are unitary, they admit identical left and right eigenvectors. Thus, Eq. (2) is equivalent to:

$$\langle \xi | B_i = \langle \xi |, \quad \forall i = 1, \dots, s. \quad (14)$$

Finally, using these properties and the decomposition in Eq. (1), we obtain:

$$\alpha|0\rangle \langle \xi | \prod_{i=1}^s B_i |\varphi\rangle = \alpha|0\rangle \langle \xi | \varphi \rangle, \quad (15)$$

$$\beta|1\rangle \langle \xi | \prod_{i=1}^s B_i A_i |\varphi\rangle = \beta|1\rangle \langle \xi | \mathcal{U} |\varphi\rangle. \quad (16)$$

Inserting Eqs. (15) and (16) into Eq. (13) yields Eq. (11), completing the proof.  $\square$

**Corollary 1.** *Let  $\mathcal{U}$  be defined as in Eqs. (1), (2) and (8). Then, the controlled application of  $\mathcal{U}^\dagger$  to an arbitrary  $n$ -qubit state  $|\varphi\rangle$ , followed by a measurement post-selected on the outcome  $|\xi\rangle$ , can be simplified as follows:*

$$\begin{aligned} \dots &= \\ |\varphi\rangle \not\perp^n \mathcal{U}^\dagger \not\perp P_\xi^\dagger \not\perp 0 &= \\ \dots &= \\ |\varphi\rangle \not\perp^n B_s^\dagger \not\perp A_s^\dagger \not\perp \dots \not\perp B_1^\dagger \not\perp A_1^\dagger \not\perp P_\xi^\dagger \not\perp 0 &= 0 \end{aligned} \quad (17)$$

*Proof.* We use Lemma 2, with  $\mathcal{U}^\dagger$  as the target unitary, which in particular admits the following decomposition:

$$\mathcal{U}^\dagger = A_1^\dagger \cdot B_1^\dagger \cdots B_s^\dagger \cdot A_s^\dagger \quad (18)$$

instead of the decomposition of  $\mathcal{U}$  given in Eq. (1). Note that since  $B_i$  are unitary, they share the same eigenstates with their adjoints  $B_i^\dagger$ , including the state  $|\xi\rangle$ .  $\square$

In the following sections, we show how these decompositions lead to substantial simplifications in several of the FOQCS-LCU's applications.

## III. THE FOQCS-LCU BLOCK ENCODING

We start by reviewing the Fast One-Qubit Controlled Select Linear Combination of Unitaries (FOQCS-LCU) block encoding proposed in [27]. In contrast to standard LCU, which expresses the target matrix as a linear combination of black-box unitaries  $U_m$  [11–25, 27, 30, 37]:

$$\mathcal{H} = \sum_{m=0}^{M-1} \alpha_m U_m, \quad \alpha_m \in \mathbb{C}, \quad (19)$$

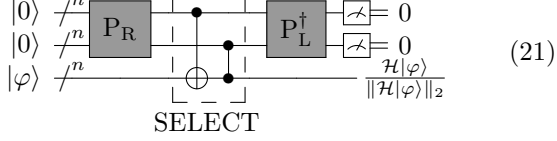
FOQCS-LCU capitalizes on a structured operator basis. Specifically, without loss of generality and in line with quantum-simulation applications, the unitaries  $U_m$  are chosen to be Pauli strings. Accordingly, we can rewrite Eq. (19) by formally separating the  $X$  and  $Z$  components of each Pauli string [23, 27, 31]:

$$\mathcal{H} = \sum_{i=0}^{2^n-1} \sum_{j=0}^{2^n-1} \sum_{\ell=0}^{n-1} \tilde{\alpha}_{ij} Z^{j_\ell} X^{i_\ell}, \quad (20)$$

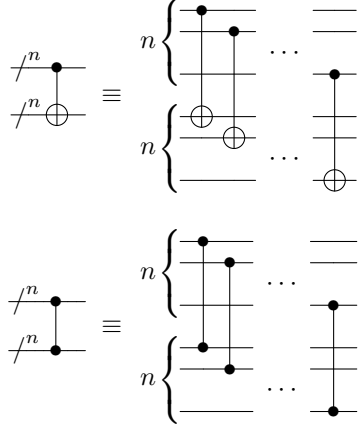
where the new coefficients  $\tilde{\alpha}_{ij}$  preserve the sparsity of the original  $\alpha_m$  and absorb an additional factor of the imaginary unit whenever  $i_\ell = j_\ell = 1$ .

### A. High-level FOQCS-LCU circuit

A fully general FOQCS-LCU block encoding circuit is given by [27]:



where the central routine, known as the SELECT oracle, consists of two parallel layers of  $n$  CNOT and  $n$  CZ gates, respectively:



In this paper, we employ a slightly different convention for the state-preparation oracles,  $P_R$  and  $P_L$ , acting on the  $2n$  ancilla qubits, compared to that in [27]. More precisely,

$$P_R |0\rangle_{2n} = \frac{1}{\sqrt{\mathcal{N}}} \sum_{i=0}^{2^n-1} \sum_{j=0}^{2^n-1} e^{i \arg(\tilde{\alpha}_{ij})} \sqrt{|\tilde{\alpha}_{ij}|} |i\rangle |j\rangle, \quad (22)$$

$$P_L |0\rangle_{2n} = \frac{1}{\sqrt{\mathcal{N}}} \sum_{i=0}^{2^n-1} \sum_{j=0}^{2^n-1} \sqrt{|\tilde{\alpha}_{ij}|} |i\rangle |j\rangle, \quad (23)$$

where phase information of the coefficients  $\tilde{\alpha}_{ij}$  is encoded solely in  $P_R$  and with an overall normalization factor:

$$\mathcal{N} = \sum_{i=0}^{2^n-1} \sum_{j=0}^{2^n-1} |\tilde{\alpha}_{ij}|. \quad (24)$$

Since the success probability of a block encoding, i.e., the probability that each ancilla qubit is measured in  $|0\rangle$ , is inversely proportional to the square of the normalization, one might be concerned that the FOQCS-LCU normalization  $\mathcal{N}$  is larger than for the standard LCU. In fact, for the standard LCU (Eq. (19)) with  $U_m$  taken to be Pauli strings, the corresponding normalization factor is precisely  $\mathcal{N}$ . Indeed, the coefficients  $\tilde{\alpha}_{ij}$  possess the same sparsity pattern as  $\alpha_m$  and differ only by phase factors.

A naive implementation of  $P_R$  and  $P_L$  amounts to preparing an arbitrary  $2n$ -qubit state, which in general entails an exponential overhead. However, by making use

of the preparation of Dicke states [38–43], we can obtain efficient implementations for a variety of Hamiltonians, including the one-dimensional Heisenberg and spin glass models [27].

### B. Controlling FOQCS-LCU

Now we apply the theory in Section II to FOQCS-LCU. In particular, we demonstrate how to control the entire block-encoding circuit by exploiting its factorization into  $P_R$ , SELECT, and  $P_L^\dagger$ . For the circuit in Eq. (21), it suffices to control only the  $P_R$  and  $P_L^\dagger$  oracles, as formalized in the following theorem.

**Theorem 1.** *Let  $\mathcal{U}_{\text{FOQCS}}$  be the unitary circuit implementing the FOQCS-LCU block encoding defined in Eq. (21). If the  $2n$  ancilla qubits are prepared in the state  $|0\rangle_{2n}$ , then the controlled application of  $\mathcal{U}_{\text{FOQCS}}$  can be simplified for any initial system state  $|\varphi\rangle$  by controlling only the  $P_R$  and  $P_L^\dagger$  oracles:*

$$|0\rangle \begin{array}{c} / \backslash^n \\ / \backslash^n \end{array} \mathcal{U}_{\text{FOQCS}} = |0\rangle \begin{array}{c} / \backslash^n \\ / \backslash^n \end{array} P_R \begin{array}{c} / \backslash^n \\ / \backslash^n \end{array} P_L^\dagger \quad (25)$$

*Proof.* We first note that, by construction, the SELECT oracle in FOQCS-LCU acts trivially on states of the form  $|0\rangle_{2n} |\varphi\rangle$ , where  $|\varphi\rangle$  is an arbitrary  $n$ -qubit state:

$$\text{SELECT} |0\rangle_{2n} |\varphi\rangle = |0\rangle_{2n} |\varphi\rangle, \quad \forall |\varphi\rangle. \quad (26)$$

That is,  $|0\rangle_{2n} |\varphi\rangle$  is an eigenstate of the SELECT unitary.

Applying Lemma 1, with  $s = 2$ , to the decomposition defined by:

$$\begin{aligned} A_1 &\equiv P_R \otimes I_n, & B_1 &\equiv \text{SELECT}, \\ A_2 &\equiv P_L^\dagger \otimes I_n, & B_2 &\equiv I_{3n}, \end{aligned} \quad (27)$$

proves Eq. (25).  $\square$

We next turn to the controlled  $P_R$  and  $P_L^\dagger$  oracles. By additionally applying Lemma 1 to these state-preparation oracles, we derive efficient controlled implementations under the assumption stated below, which is satisfied by all  $P_R$  and  $P_L$  oracles in both [27] and Section V.

**Assumption 1.** *The oracles  $P_R$  and  $P_L$  admit unitary decompositions of the form:*

$$P_R \equiv \tilde{P}_R \cdot A_R, \quad P_L \equiv \tilde{P}_L \cdot A_L, \quad (28)$$

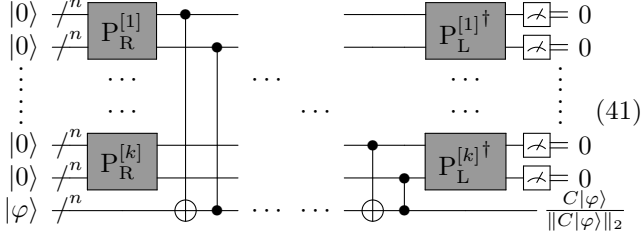
where  $\tilde{P}_R$  and  $\tilde{P}_L$  have the all-zero state  $|0\rangle_{2n}$  as an eigenstate corresponding to the eigenvalue 1:

$$\tilde{P}_R |0\rangle_{2n} = |0\rangle_{2n}, \quad \tilde{P}_L |0\rangle_{2n} = |0\rangle_{2n}, \quad (29)$$

and  $A_R$  and  $A_L$  consist of only  $\mathcal{O}(1)$  single-qubit gates.



and a block encoding of  $C$  can be realized by the circuit:

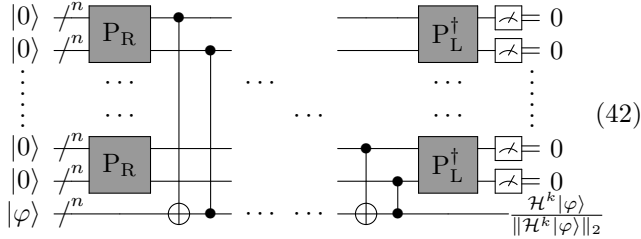


where  $P_R^{[s]}$  and  $P_L^{[s]\dagger}$  denote the state-preparation oracles defined in Eqs. (22) and (23), associated with the FOQCS-LCU block encodings of  $\{M_s\}_{s=1}^k$ .

*Proof.* The proof is a straightforward generalization of Theorem 2 and differs only in the inclusion of additional index sets.  $\square$

Finally, we show how Corollary 3 applies in the specific case of block encodings of powers of  $\mathcal{H}$ .

**Corollary 4.** *Let  $\mathcal{H}$  be a matrix expressed as a linear combination of Pauli strings, as in Eq. (20). Then, a block encoding of  $\mathcal{H}^k$  can be realized by the circuit:*



where  $P_R$  and  $P_L$  are defined in Eqs. (22) and (23) and are performed, in parallel,  $k$  times.

*Proof.* This corollary can be viewed as a special case of Corollary 3, where  $M_s \equiv \mathcal{H}$ , for  $s = 1, \dots, k$ .  $\square$

## B. Block encodings for matrix polynomials

Given block encodings of the matrix powers  $\mathcal{H}^k$ , we now build a FOQCS-LCU-type block encoding for their linear combination. Concretely, we consider a degree- $d$  matrix polynomial in  $\mathcal{H}$ :

$$p_d(\mathcal{H}) = a_0 I + a_1 \mathcal{H} + a_2 \mathcal{H}^2 + \dots + a_d \mathcal{H}^d, \quad (43)$$

with coefficients  $a_k \in \mathbb{C}$  for  $k = 0, 1, \dots, d$ .

To realize an efficient block encoding for  $p_d(\mathcal{H})$  under the FOQCS-LCU framework, we embed the block encodings of  $\mathcal{H}^k$  within a second LCU layer. This *outer* LCU procedure requires the state-preparation oracles  $\text{POLY}_R$  and  $\text{POLY}_L$  to encode the coefficients  $a_k$ , as well as a SELECT oracle to activate the corresponding powers of  $\mathcal{H}$ . Crucially, instead of using the standard approach to implement the outer LCU, which would require  $\lceil \log_2(d) \rceil$  ancilla qubits, we load the coefficients  $a_k$  through a *unary encoding* [14, 36] on  $d$  ancilla qubits. As a consequence,

we again avoid multi-controlled unitaries in the SELECT operation for  $\mathcal{H}^k$ .

We first introduce the weighted coefficients associated with the matrix polynomial coefficients  $a_k$ :

$$w_k := \sqrt{|a_k| \mathcal{N}^k}, \quad (44)$$

where  $\mathcal{N}$  denotes the FOQCS-LCU normalization factor defined in Eq. (24). Next, for  $k = 0, \dots, d-1$ , we define the relative phase differences

$$\phi_k := \arg(a_{k+1}) - \arg(a_k), \quad (45)$$

and introduce the angles

$$\theta_k := 2 \arccos \left( \frac{|w_k|}{\sqrt{1 - \sum_{p=0}^{k-1} |w_p|^2}} \right). \quad (46)$$

We then define the outer state-preparation oracles,  $\text{POLY}_R$  and  $\text{POLY}_L$ , respectively, as follows.

**Definition 1.** *Let  $a_k \in \mathbb{C}$ , for  $k = 0, 1, \dots, d$ , be the coefficients of the matrix polynomial in Eq. (43), and  $w_k$  and  $\phi_k$  the associated set of real parameters defined in Eqs. (44) and (45). Then, we can define the  $d$ -qubit outer state-preparation oracles<sup>1</sup>:*

$$\text{POLY}_R |0\rangle_d = \frac{1}{\sqrt{\mathcal{W}}} \sum_{k=0}^d e^{i \sum_{j=0}^{k-1} \phi_j} w_k |k_u\rangle, \quad (47)$$

$$\text{POLY}_L |0\rangle_d = \frac{1}{\sqrt{\mathcal{W}}} \sum_{k=0}^d w_k |k_u\rangle, \quad (48)$$

where  $\mathcal{W}$  is a normalization factor:

$$\mathcal{W} = \sum_{k=0}^d w_k^2 = \sum_{k=0}^d |a_k| \mathcal{N}^k, \quad (49)$$

and  $|k_u\rangle$  the unary encoding of the index  $k$ , i.e.:

$$\begin{aligned} |0_u\rangle &= |000 \dots 0\rangle, \\ |1_u\rangle &= |100 \dots 0\rangle, \\ |2_u\rangle &= |110 \dots 0\rangle, \\ &\vdots \\ |d_u\rangle &= |111 \dots 1\rangle. \end{aligned} \quad (50)$$

We also define the following  $d$ -qubit circuits that will serve as essential subroutines for realizing the two state-

<sup>1</sup> When  $k = 0$ , we take  $\sum_{j=0}^{-1} \phi_j = 0$ .

preparation oracles  $\text{POLY}_R$  and  $\text{POLY}_L$ :

$$\frac{1}{\sqrt{d}} \text{CR}_y(\theta_1^{d-1}) = \begin{array}{c} \dots \\ | \quad | \\ \text{R}_y(\theta_1) \quad \text{R}_y(\theta_2) \\ | \quad | \\ \dots \end{array} \quad (51)$$

$$\frac{1}{\sqrt{d}} \text{P}(\phi_0^{d-1}) = \begin{array}{c} \dots \\ | \quad | \\ \text{P}(\phi_0) \quad \text{P}(\phi_1) \\ | \quad | \\ \vdots \\ | \quad | \\ \text{P}(\phi_{d-1}) \end{array} \quad (52)$$

where rotation and phase gates follow the conventions:

$$\text{R}_y(\theta) = \begin{pmatrix} \cos(\frac{\theta}{2}) & -\sin(\frac{\theta}{2}) \\ \sin(\frac{\theta}{2}) & \cos(\frac{\theta}{2}) \end{pmatrix}, \quad \text{P}(\phi) = \begin{pmatrix} 1 & 0 \\ 0 & e^{i\phi} \end{pmatrix}. \quad (53)$$

Using Eqs. (51) and (52), we can efficiently implement the  $\text{POLY}_R$  oracle to generate a weighted superposition over unary-encoded indices, as originally proposed in [28] and summarized in the following lemma.

**Lemma 3.** *The state-preparation oracle  $\text{POLY}_R$ , defined in Eq. (47), can be realized by the  $d$ -qubit circuit:*

$$\frac{1}{\sqrt{d}} \text{POLY}_R = \begin{array}{c} | \quad | \\ \text{R}_y(\theta_0) \quad \text{CR}_y(\theta_1^{d-1}) \quad \text{P}(\phi_0^{d-1}) \\ | \quad | \\ \dots \end{array} \quad (54)$$

where the rotation angles  $\theta_k$  and the phase angles  $\phi_k$  are given in Eq. (46) and Eq. (45), respectively.

Similarly, we can efficiently implement the  $\text{POLY}_L$  oracle, as stated in the following lemma.

**Lemma 4.** *The state-preparation oracle  $\text{POLY}_L$ , defined in Eq. (48), can be realized by the  $d$ -qubit circuit:*

$$\frac{1}{\sqrt{d}} \text{POLY}_L = \begin{array}{c} | \quad | \\ \text{R}_y(\theta_0) \quad \text{CR}_y(\theta_1^{d-1}) \\ | \quad | \\ \dots \end{array} \quad (55)$$

where the rotation angles  $\theta_k$  are given in Eq. (46).

We remark that the  $\text{POLY}_R$  and  $\text{POLY}_L$  circuits given in Lemmas 3 and 4, respectively, each require only  $2(d-1)$  CNOT gates following Eq. (51).

Finally, by combining the outer state-preparation oracles  $\text{POLY}_R$  and  $\text{POLY}_L$ , defined in Definition 1 and implemented as described in Lemmas 3 and 4, together with the constructions from Section IV A, we obtain an efficient block encoding of the matrix polynomial  $p_d(\mathcal{H})$ , as formalized in the following theorem.

**Theorem 3.** *Let  $p_d(\mathcal{H})$  be a degree- $d$  matrix polynomial in an  $n$ -qubit matrix  $\mathcal{H}$ , as defined within Eq. (43). Then, the  $(d + (2d + 1)n)$ -qubit circuit shown in Fig. 1a implements a block encoding of  $p_d(\mathcal{H})$ .*

*Proof.* See Section B.  $\square$

The circuit in Fig. 1a is fully general and applies to any matrix  $\mathcal{H}$  implemented through the FOQCS-LCU block encoding. In principle, controlling the associated state-preparation oracles can incur a significant overhead. However, the circuit identities in Eqs. (30) and (31) show that the controlled  $\text{P}_R$  and  $\text{P}_L^\dagger$  oracles can be simplified if Assumption 1 is valid, leading to the simplified construction of the following corollary.

**Corollary 5.** *If  $\text{P}_R$  and  $\text{P}_L$  satisfy Assumption 1, the block-encoding circuit in Fig. 1a admits the simplification shown in Fig. 1b.*

*Proof.* The circuit in Fig. 1b follows directly from Fig. 1a, assuming  $\text{P}_R$  and  $\text{P}_L^\dagger$  satisfy Assumption 1.  $\square$

### C. Controlling the matrix polynomial of $\mathcal{H}$

To control the entire circuits implementing  $p_d(\mathcal{H})$  shown in Fig. 1, we start with the following two lemmas, which detail how to efficiently control the  $\text{POLY}_R$  and  $\text{POLY}_L$  circuits.

**Lemma 5.** *Let the  $\text{POLY}_R$  circuit be defined as in Lemma 3. Then, controlling the entire  $\text{POLY}_R$  requires controlling only the first  $\text{R}_y$  gate when we apply the gate to the  $|0\rangle_d$  state:*

$$|0\rangle \frac{1}{\sqrt{d}} \text{POLY}_R = \begin{array}{c} | \quad | \\ |0\rangle \text{R}_y(\theta_0) \quad \text{CR}_y(\theta_1^{d-1}) \quad \text{P}(\phi_0^{d-1}) \\ | \quad | \\ |0\rangle \quad \dots \end{array} \quad (56)$$

*Proof.* The  $\text{POLY}_R$  unitary can be decomposed using Lemma 1 with  $s = 1$ . In particular, from the circuit implementation in Eq. (54), we can isolate the first  $\text{R}_y$  rotation, since the remaining part of the circuit has  $|0\rangle_d$  as an eigenstate with eigenvalue 1.  $\square$

**Lemma 6.** *Let the  $\text{POLY}_L$  circuit be defined as in Lemma 4. Then, controlling the entire  $\text{POLY}_L^\dagger$  requires controlling only the last  $\text{R}_y$  gate when we measure all the*

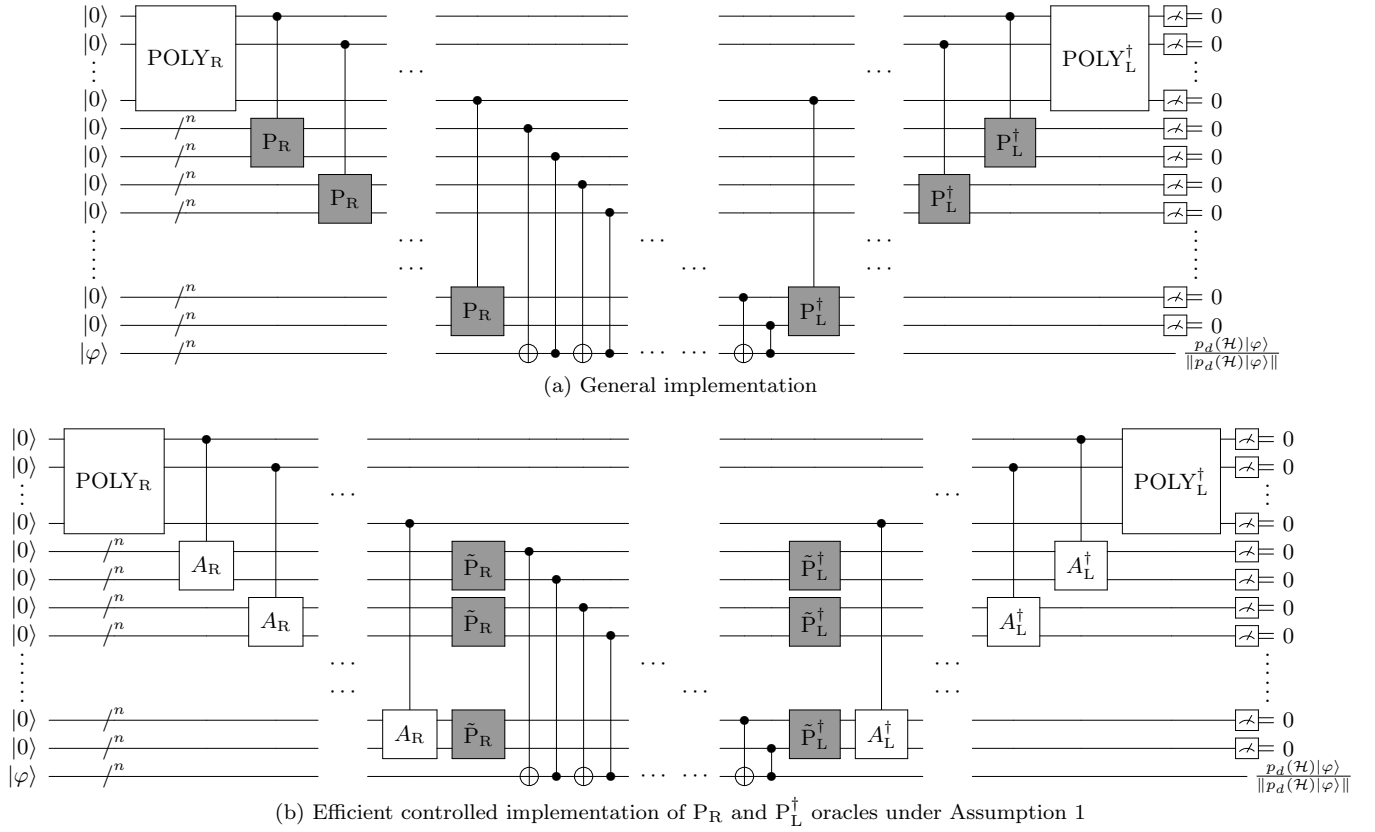
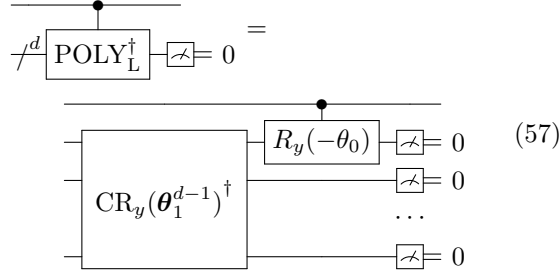


Figure 1: FOQCS-LCU block encoding circuits for a matrix polynomial  $p_d(\mathcal{H}) = a_0I + a_1\mathcal{H} + a_2\mathcal{H}^2 + \dots + a_d\mathcal{H}^d$ .

bottom  $d$  qubits in the  $|0\rangle_d$  state:



*Proof.* The  $\text{POLY}_L^\dagger$  unitary can be decomposed using Corollary 1 with  $s = 1$ . By considering the adjoint circuit of Eq. (55), we can isolate the last  $R_y$  rotation in  $\text{POLY}_L^\dagger$ , since the remaining part of the circuit has  $|0\rangle_d$  as an eigenstate with eigenvalue 1.  $\square$

Consequently, controlling the entire matrix polynomial circuit requires controlling only these boundary  $R_y$  rotations. This is summarized in the following theorem.

**Theorem 4.** *Let  $p_d(\mathcal{H})$  be the matrix polynomial defined in Eq. (43), and consider both the general and simplified block encoding circuits shown in Fig. 1. For either implementation, controlling the entire circuit is equivalent to controlling only the first and last  $R_y$  rotations of  $\text{POLY}_R$  and  $\text{POLY}_L^\dagger$ , respectively.*

*Proof.* First, we note that in order to control the entire circuit, it suffices to control only the  $\text{POLY}_R$  and  $\text{POLY}_L^\dagger$  oracles defined in Definition 1. Indeed, if these oracles are not activated, the controlled  $P_R$  and  $P_L^\dagger$  gates are not applied, since they have  $|0\rangle_d$  as the control state, and the entire circuit thus acts trivially on the state  $|0\rangle_d |0\rangle_{2n} |\varphi\rangle$ . Then we apply Lemmas 5 and 6, such that both circuits in Fig. 1 can be controlled by simply controlling the first and last  $R_y$  rotation gates within  $\text{POLY}_R$  and  $\text{POLY}_L^\dagger$ , respectively. This completes the proof.  $\square$

We conclude by remarking that a  $R_y$  gate can be implemented with up to 2 CNOT gates. As a result, all matrix polynomial block encodings defined in Section IV B can be controlled with a trivial overhead of 4 CNOTs.

## V. APPLICATIONS

As discussed in the previous sections, the circuit depth of controlled FOQCS-LCU block encodings can be significantly reduced when Assumption 1 is satisfied. In particular, decomposing the  $P_R$  and  $P_L^\dagger$  oracles into two components—one consisting solely of  $\mathcal{O}(1)$  single-qubit gates and another for which the all-zero state  $|0\rangle_{2n}$  is an eigenstate—enables substantial simplifications of controlled FOQCS-LCU circuits. While these conditions are

Circuit	CNOT count		CNOT depth		Number of qubits	
	all-to-all	square grid	all-to-all	square grid	all-to-all	square grid
P <sub>R</sub> /P <sub>L</sub> Controlled-P <sub>R</sub> /P <sub>L</sub>	11n - 11	11n - 7	4n + 4	4n + 8	2n	2n
	11n - 10	11n - 6	4n + 5	4n + 9	2n + 1	2n + 1
FOQCS-LCU Controlled-FOQCS-LCU	24n - 22	26n - 14	8n + 10	8n + 20	3n	3n
	24n - 20	26n - 12	8n + 12	8n + 22	3n + 1	3n + 1
p <sub>d</sub> (H) Controlled-p <sub>d</sub> (H)	24dn - 18d - 4	26dn - 2d - 6	8n + 6d + 6	8n + 10d + 12	2dn + d + n	2dn + 2d + n
	24dn - 18d	26dn - 2d - 2	8n + 6d + 10	8n + 10d + 16	2dn + d + n + 1	2dn + 2d + n + 1

Table I: Resource analysis for the P<sub>R</sub> and P<sub>L</sub><sup>†</sup> oracles, the FOQCS-LCU block encoding, a generic matrix polynomial of H and their controlled circuits for the one-dimensional XYZ Heisenberg Hamiltonian defined in Eq. (58).

not met by arbitrary state-preparation routines, they do hold for all block encodings introduced in [27], making these simplifications practically achievable.

Motivated by this observation, we focus in this section on representative one-dimensional spin Hamiltonians. In Section V A we present explicit decompositions of P<sub>R</sub> and P<sub>L</sub><sup>†</sup>. These decompositions require negligible overhead for controlling the FOQCS-LCU circuits and allow for substantial simplifications in the implementation of matrix polynomials. We then present the Hadamard test as a representative application of controlled FOQCS-LCU circuits in Section V B. Finally, we demonstrate applications of matrix polynomial circuits to time evolution in Section V C.

### A. Explicit circuits for spin Hamiltonians

Let us consider the one-dimensional XYZ Heisenberg Hamiltonian with open boundary conditions:

$$\mathcal{H} = g \sum_{i=0}^{n-1} Z_i + \sum_{i=0}^{n-2} J_x X_i X_{i+1} + J_y Y_i Y_{i+1} + J_z Z_i Z_{i+1}. \quad (58)$$

Note that more general field terms  $\sum_i g_x X_i + g_y Y_i + g_z Z_i$ , as considered in [27], can be rotated to the Z-axis through a single global change of spin coordinates. Without loss of generality, we may therefore choose  $g_x = g_y = 0$  and  $g_z = g$ . We exploit this simplification in the Hamiltonian definition to further compress the P<sub>R</sub> and P<sub>L</sub> oracles from [27]. In particular, Fig. 2 illustrates the optimized P<sub>R</sub> oracle for  $n = 4$  spins, while Section C1 provides a detailed construction for general  $n$ .

Crucially, the P<sub>R</sub> oracle from Fig. 2 satisfies Assumption 1 and can be decomposed into two parts by isolating the first X gate from the remainder of the circuit:

$$\begin{array}{c} \text{P}_R \\ \vdots \end{array} \equiv \begin{array}{c} X \\ \dots \\ \text{P}_R \end{array} \quad (59)$$

Because  $\tilde{P}_R$  contains only controlled gates, it has eigenstate  $|0\rangle_{2n}$  with eigenvalue 1. As a consequence, Eq. (30)

yields:

$$\begin{array}{c} |0\rangle \\ |0\rangle \\ \vdots \\ |0\rangle \end{array} \text{P}_R = \begin{array}{c} |0\rangle \\ |0\rangle \\ \vdots \\ |0\rangle \end{array} \begin{array}{c} X \\ \dots \\ \tilde{P}_R \end{array} \quad (60)$$

Controlling the XYZ Heisenberg P<sub>R</sub> oracle thus incurs a trivial overhead, namely *a single additional CNOT gate*. Analogously, Assumption 1 and Eq. (31) also apply to the simplification of the controlled P<sub>L</sub><sup>†</sup> gate:

$$\begin{array}{c} \text{P}_L^\dagger \\ \vdots \\ \text{P}_L^\dagger \end{array} \begin{array}{c} \text{X} \\ \vdots \\ \text{X} \end{array} = \begin{array}{c} \tilde{P}_L^\dagger \\ \vdots \\ \tilde{P}_L^\dagger \end{array} \begin{array}{c} X \\ \vdots \\ X \end{array} \quad (61)$$

In Table I, we evaluate the non-asymptotic resource cost for this model, for which Eq. (60) and Eq. (61) hold. To derive the circuit depth and CNOT count, we consider both all-to-all and square-grid qubit connectivity. We observe that the circuit implemented on a two-dimensional grid has nearly the same complexity as the all-to-all connectivity case. This is made possible by an appropriate mapping of qubits onto the two-dimensional grid, which allows us to effectively exploit horizontal and vertical nearest-neighbor qubit interactions. In particular, Section D details the implementation of two-dimensional FOQCS-LCU circuits on a square grid.

In addition to the XYZ Heisenberg model, we explicitly provide the P<sub>R</sub> circuits for the XXZ and Ising models in Section C. In both cases, the decomposition in Eq. (59) applies, as do the corresponding simplifications for the controlled circuits in Eqs. (60) and (61).

The consequences of this simplification are significant: for a broad class of spin models considered here and in [27], controlling the full FOQCS-LCU block encoding incurs the cost of *only two additional CNOT gates*, as illustrated in Fig. 3. Moreover, the circuit implementing a matrix polynomial of H admits a substantial simplification as well: control of each A<sub>R</sub> or A<sub>L</sub><sup>†</sup> gate in Fig. 1b introduces only a single CNOT gate. For concreteness, Fig. 4 shows the total CNOT depth required to implement matrix polynomials of increasing degree for the XYZ model.

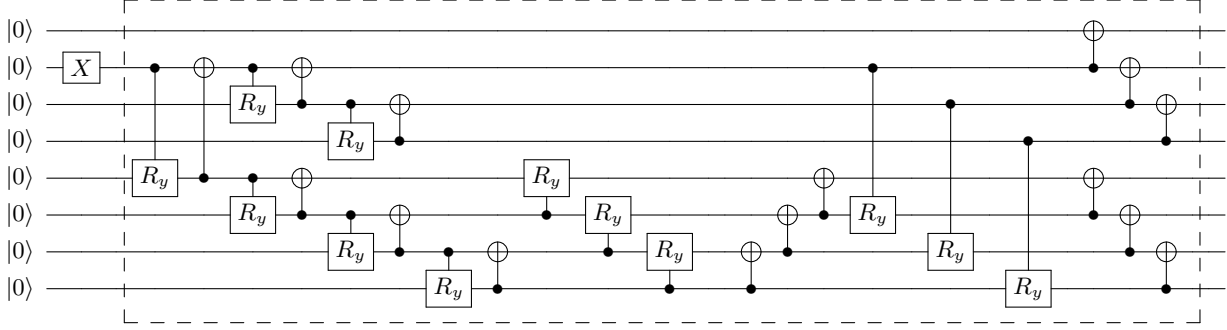


Figure 2: Simplified  $P_R$  circuit for the one-dimensional XYZ Heisenberg Hamiltonian with open boundary conditions, defined in Eq. (58), for the case  $n = 4$ . The dashed region corresponds to the gate  $\tilde{P}_R$  in Assumption 1.

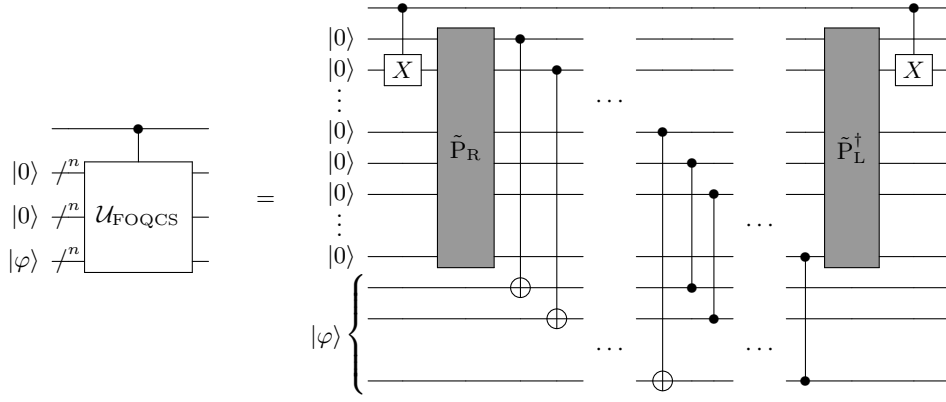


Figure 3: Circuit implementing the controlled FOQCS-LCU block encoding of  $\mathcal{H}$ .

Finally, for completeness, a full and explicit circuit implementing a matrix polynomial of the Ising Hamiltonian is included in Section E for  $n = 3$  and  $d = 3$ .

### B. Hadamard tests

The Hadamard test is a canonical method to estimate the expectation value  $\langle \varphi | \mathcal{U} | \varphi \rangle$  of a unitary  $\mathcal{U}$  in a state  $|\varphi\rangle$ . This is achieved by controlling  $\mathcal{U}$  and then measuring an ancilla qubit:  $X$ -basis measurements yield  $\text{Re} \langle \varphi | \mathcal{U} | \varphi \rangle$  and  $Y$ -basis measurements  $\text{Im} \langle \varphi | \mathcal{U} | \varphi \rangle$ . The corresponding Hadamard-test circuit for extracting the real part is

$$|0\rangle \xrightarrow{\mathcal{U}} \begin{array}{c} H \\ \diagup \quad \diagdown \\ H \end{array} \xrightarrow{\mathcal{U}} \text{Re} \langle \varphi | \mathcal{U} | \varphi \rangle \quad (62)$$

where  $H$  is the Hadamard gate. In the case of a non-unitary operator  $\mathcal{H}$ , we can still perform the Hadamard test by controlling the entire block encoding circuit while initializing and post-selecting the FOQCS-LCU ancilla

qubits in the state  $|0\rangle_{2n}$ :

$$|0\rangle \xrightarrow{\mathcal{U}} \begin{array}{c} H \\ \diagup \quad \diagdown \\ H \end{array} \xrightarrow{\mathcal{U}} \text{Re} \langle \varphi | \mathcal{H} | \varphi \rangle \quad (63)$$

$$|0\rangle \xrightarrow{\mathcal{U}} \begin{array}{c} H \\ \diagup \quad \diagdown \\ H \end{array} \xrightarrow{\mathcal{U}} 0$$

$$|0\rangle \xrightarrow{\mathcal{U}} \begin{array}{c} H \\ \diagup \quad \diagdown \\ H \end{array} \xrightarrow{\mathcal{U}} 0$$

This yields the desired  $\text{Re} \langle \varphi | \mathcal{H} | \varphi \rangle$ .

In general, controlling a block encoding of  $\mathcal{H}$  incurs significant overhead. In Section III B, however, we show that this overhead can be substantially reduced for the FOQCS-LCU block encoding when the state-preparation oracles satisfy Assumption 1. Specifically, in Section V A we demonstrate that this assumption holds for the one-dimensional XYZ Heisenberg model. It likewise holds for the XXZ and Ising models, as verified in Sections C2 and C3. In all these cases, controlling the block encoding of  $\mathcal{H}$  costs only two additional CNOT gates.

As a result, FOQCS-LCU is particularly well suited for Hadamard-test-based applications. Figure 5 summarizes the resources required to implement a Hadamard test for each considered spin Hamiltonian, for both all-to-all and square-grid connectivity architectures. We observe that,

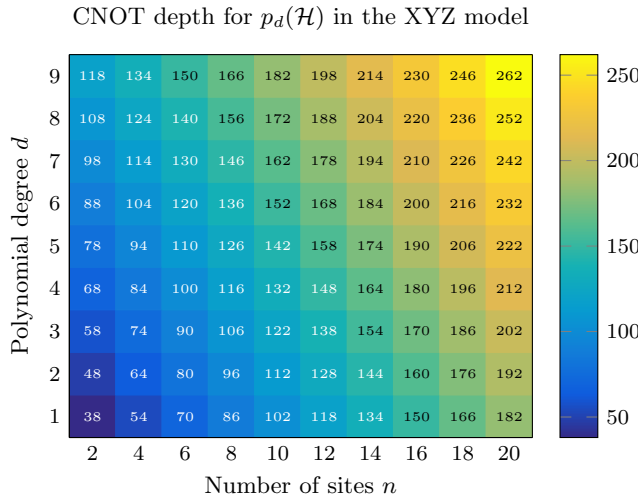


Figure 4: Total CNOT depth for implementing the matrix polynomial  $p_d(\mathcal{H})$  of the one-dimensional XYZ Heisenberg Hamiltonian as a function of system size  $n$  and polynomial degree  $d$ , assuming a square-grid connectivity (See Table I).

in all cases, both the CNOT count and CNOT depth for the block encoding circuits scale linearly with the system size  $n$ . Moreover, moving from all-to-all to square-grid connectivity incurs only a modest overhead; in fact, the circuit-depth overhead is constant.

### C. Time evolution and Loschmidt echo

A direct application of matrix polynomial transformations is the approximation of the time-evolution operator by a degree- $d$  polynomial,

$$e^{-i\mathcal{H}t} \approx p_d(\mathcal{H}) = \sum_{k=0}^d c_k \mathcal{H}^k, \quad (64)$$

which can be obtained, for instance, through a Taylor or Chebyshev expansion.

Additionally, the Hadamard tests can be applied to the time evolution operator to measure the Loschmidt echo  $g(t) = \langle \varphi | e^{-i\mathcal{H}t} | \varphi \rangle$ :

$$\begin{array}{c} |0\rangle \xrightarrow{H} \bullet \xrightarrow{H} \text{Re}(g(t)) \\ |\varphi\rangle \xrightarrow{/n} e^{-i\mathcal{H}t} \end{array} \quad (65)$$

The circuit above constitutes a core component of many hardware-efficient quantum phase estimation (QPE) methods [44–49].

With the approximation of Eq. (64), we can estimate  $g(t) \approx \langle \varphi | p_d(\mathcal{H}) | \varphi \rangle$  by controlling the block encoding of the matrix polynomial  $p_d(\mathcal{H})$  while initializing and post-selecting all ancilla qubits in the state  $|0\rangle_{2dn}$ , similarly to

Eq. (63):

$$\begin{array}{c} |0\rangle \xrightarrow{H} \bullet \xrightarrow{H} \text{Re} \langle \varphi | p_d(\mathcal{H}) | \varphi \rangle \\ |0\rangle \xrightarrow{2dn} p_d(\mathcal{H}) \xrightarrow{/n} \text{Re} \langle \varphi | p_d(\mathcal{H}) | \varphi \rangle = 0 \\ |\varphi\rangle \xrightarrow{/n} \end{array} \quad (66)$$

In Section IV C, we establish that controlling the circuit implementing  $p_d(\mathcal{H})$  incurs only a trivial overhead of four additional CNOT gates. Consequently, the FOQCS-LCU block encoding can substantially reduce the control cost associated with QPE routines, therefore improving their feasibility on near-term quantum hardware.

## VI. CONCLUSIONS

By leveraging the FOQCS-LCU formalism, we have shown that matrix polynomial transformations can be implemented with a CNOT-depth overhead that is only linear in the polynomial degree  $d$ , and independent of both the system size  $n$  and the cost of block encoding the original matrix. For the spin models considered here, this results in an overall CNOT depth scaling as the sum  $c_1 n + c_2 d$ , with small integer coefficients  $c_1$  and  $c_2$ . By contrast, a QSVD-based implementation for the same systems would entail a circuit depth proportional to the product  $d \cdot n$ .

This substantial reduction in circuit depth comes at an expense of additional ancilla qubits. While this trade-off must be taken into account, it aligns well with the current trends in quantum hardware development: qubit counts continue to increase steadily, whereas achievable circuit depth remains a primary bottleneck due to noise and coherence constraints. From this perspective, prioritizing shallow and highly parallelizable circuits is often more practical than minimizing the total qubit count.

Moreover, we have shown that both the FOQCS-LCU block encoding and the associated matrix polynomial circuits can be controlled with negligible overhead. In particular, a Hadamard test applied to a FOQCS-LCU block encoding requires only 2 extra CNOT gates, while a Hadamard test applied to a matrix polynomial implemented using FOQCS-LCU incurs the overhead of just 2 controlled single-qubit rotations, corresponding to a total of 4 extra CNOT gates.

For all applications considered, we provide explicit circuit constructions, including qubit mappings for two-dimensional square-grid architectures, and we show that the additional circuit depth incurred by this connectivity constraint remains constant with respect to the system size.

The circuits and techniques introduced in this paper are broadly applicable to problems across quantum simulation and quantum linear algebra, and are not limited to the specific physical models considered here. Furthermore, the resulting circuit depths and qubit requirements bring several of these constructions within reach of current and near-term quantum hardware. In doing so, our

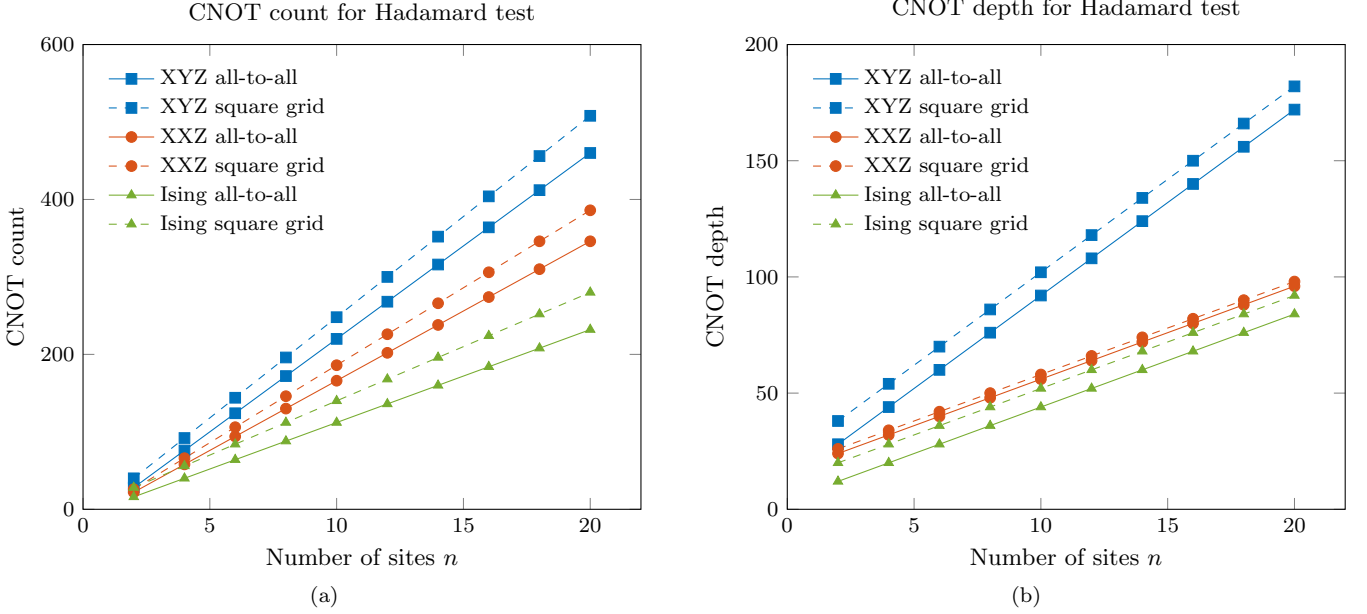


Figure 5: CNOT count (a) and depth (b) for a circuit implementing the Hadamard test, defined in Eq. (62). The computational cost for preparing the state  $|\varphi\rangle$  is excluded. We consider the one-dimensional XYZ and XXZ Heisenberg models as well as the Ising model, with computational costs detailed in Tables I to III.

framework opens the door to practical implementations of block-encoding-based algorithms that have, until now, remained largely theoretical due to prohibitive resource demands.

#### ACKNOWLEDGMENTS

MN acknowledges funding by the Munich Quantum Valley, section K5 Q-DESSI. The research is part of

the Munich Quantum Valley, which is supported by the Bavarian state government with funds from the Hightech Agenda Bayern Plus. This research is supported by the U.S. Department of Energy, Office of Science, Accelerated Research in Quantum Computing, Fundamental Algorithmic Research toward Quantum Utility (FAR-Qu).

---

[1] Y. Dong and L. Lin, Random circuit block-encoded matrix and a proposal of quantum linpack benchmark, *Phys. Rev. A* **103**, 062412 (2021).

[2] D. Camps and R. Van Beeumen, FABLE: Fast approximate quantum circuits for block-encodings, in *2022 IEEE International Conference on Quantum Computing and Engineering (QCE)* (2022) pp. 104–113.

[3] Q. T. Nguyen, B. T. Kiani, and S. Lloyd, Block-encoding dense and full-rank kernels using hierarchical matrices: applications in quantum numerical linear algebra, *Quantum* **6**, 876 (2022).

[4] D. Camps, L. Lin, R. Van Beeumen, and C. Yang, Explicit quantum circuits for block encodings of certain sparse matrices, *SIAM J. Matrix Anal. Appl.* **45**, 801 (2024).

[5] C. Sünderhauf, E. Campbell, and J. Camps, Block-encoding structured matrices for data input in quantum computing, *Quantum* **8**, 1226 (2024).

[6] P. Kuklinski and B. Rempfer, S-FABLE and LS-FABLE: Fast approximate block-encoding algorithms for unstructured sparse matrices (2024), [arXiv:2401.04234](https://arxiv.org/abs/2401.04234).

[7] P. Kuklinski, B. Rempfer, J. Elenewski, and K. Obenland, Efficient block-encodings require structure (2025), [arXiv:2509.19667](https://arxiv.org/abs/2509.19667).

[8] M. Nibbi and C. B. Mendl, Block encoding of matrix product operators, *Phys. Rev. A* **110**, 042427 (2024).

[9] L. Rullkötter, S. Weber, V. M. Katukuri, C. Tutschku, and B. C. Mummaneni, Resource-efficient variational block-encoding (2025), [arXiv:2507.17658](https://arxiv.org/abs/2507.17658).

[10] D. Liu, W. Du, L. Lin, J. P. Vary, and C. Yang, An efficient quantum circuit for block encoding a pairing Hamiltonian, *J. Comput. Sci.* **85**, 102480 (2025).

[11] A. M. Childs and N. Wiebe, Hamiltonian simulation using linear combinations of unitary operations, *Quantum Inf. Comput.* **12**, 0901 (2012).

[12] A. M. Childs, D. Maslov, Y. Nam, N. J. Ross, and Y. Su, Toward the first quantum simulation with quan-

tum speedup, *Proc. Natl. Acad. Sci. U.S.A.* **115**, 9456 (2018).

[13] A. Gilyén, Y. Su, G. H. Low, and N. Wiebe, Quantum singular value transformation and beyond: exponential improvements for quantum matrix arithmetics, in *Proceedings of the 51st Annual ACM SIGACT Symposium on Theory of Computing* (2019) pp. 193–204.

[14] R. Babbush, C. Gidney, D. W. Berry, N. Wiebe, J. McClean, A. Paler, A. Fowler, and H. Neven, Encoding electronic spectra in quantum circuits with linear T complexity, *Phys. Rev. X* **8**, 041015 (2018).

[15] R. Babbush, D. W. Berry, J. R. McClean, and H. Neven, Quantum simulation of chemistry with sublinear scaling in basis size, *npj Quantum Inf.* **5**, 92 (2019).

[16] Y. R. Sanders, D. W. Berry, P. C. Costa, L. W. Tessler, N. Wiebe, C. Gidney, H. Neven, and R. Babbush, Compilation of fault-tolerant quantum heuristics for combinatorial optimization, *PRX Quantum* **1**, 020312 (2020).

[17] J. Lee, D. W. Berry, C. Gidney, W. J. Huggins, J. R. McClean, N. Wiebe, and R. Babbush, Even more efficient quantum computations of chemistry through tensor hypercontraction, *PRX Quantum* **2**, 030305 (2021).

[18] K. Wan, Exponentially faster implementations of Select(H) for fermionic Hamiltonians, *Quantum* **5**, 380 (2021).

[19] G. Boyd, Low-overhead parallelisation of LCU via commuting operators (2024), [arXiv:2312.00696](https://arxiv.org/abs/2312.00696).

[20] I. Loaiza, A. Sankar Brahmachari, and A. F. Izmaylov, Majorana tensor decomposition: a unifying framework for decompositions of fermionic Hamiltonians to linear combination of unitaries, *Quantum Sci. Technol.* **10**, 035035 (2025).

[21] S. Chakraborty, Implementing any linear combination of unitaries on intermediate-term quantum computers, *Quantum* **8**, 1496 (2024).

[22] C. F. Kane, S. Hariprakash, N. S. Modi, M. Kreshchuk, and C. W. Bauer, Block encoding bosons by signal processing, *Quantum* **9**, 1747 (2025).

[23] T. N. Georges, M. Bothe, C. Sünderhauf, B. K. Berntson, R. Izsák, and A. V. Ivanov, Quantum simulations of chemistry in first quantization with any basis set, *npj Quantum Inf.* **11**, 55 (2025).

[24] W. A. Simon, C. M. Gustin, K. Serafin, A. Ralli, G. R. Goldstein, and P. J. Love, Ladder operator block-encoding (2025), [arXiv:2503.11641](https://arxiv.org/abs/2503.11641).

[25] D. Liu, S. Zhu, G. H. Low, L. Lin, and C. Yang, Block encoding with low gate count for second-quantized Hamiltonians (2025), [arXiv:2510.08644](https://arxiv.org/abs/2510.08644).

[26] N. Schillo, A. Sturm, and R. Quay, Block encoding linear combinations of Pauli strings using the stabilizer formalism (2026), [arXiv:2601.05740](https://arxiv.org/abs/2601.05740).

[27] F. Della Chiara, M. Nibbi, Y. Shen, and R. Van Beeumen, Efficient LCU block encodings through Dicke states preparation (2025), [arXiv:2507.20887](https://arxiv.org/abs/2507.20887).

[28] D. W. Berry, A. M. Childs, R. Cleve, R. Kothari, and R. D. Somma, Simulating Hamiltonian dynamics with a truncated Taylor series, *Phys. Rev. Lett.* **114**, 090502 (2015).

[29] R. Meister, S. C. Benjamin, and E. T. Campbell, Tailoring term truncations for electronic structure calculations using a linear combination of unitaries, *Quantum* **6**, 637 (2022).

[30] M. W. Sze, Y. Tang, S. Dilkes, D. M. Ramo, R. Duncan, and N. Fitzpatrick, Hamiltonian dynamics simulation using linear combination of unitaries on an ion trap quantum computer (2025), [arXiv:2501.18515](https://arxiv.org/abs/2501.18515).

[31] W. Kirby, M. Motta, and A. Mezzacapo, Exact and efficient Lanczos method on a quantum computer, *Quantum* **7**, 1018 (2023).

[32] G. H. Low and I. L. Chuang, Hamiltonian simulation by qubitization, *Quantum* **3**, 163 (2019).

[33] J. M. Martyn, Z. M. Rossi, A. K. Tan, and I. L. Chuang, Grand unification of quantum algorithms, *PRX Quantum* **2**, 040203 (2021).

[34] Y. Kikuchi, C. Mc Keever, L. Coopmans, M. Lubasch, and M. Benedetti, Realization of quantum signal processing on a noisy quantum computer, *npj Quantum Inf.* **9**, 93 (2023).

[35] D. Motlagh and N. Wiebe, Generalized quantum signal processing, *PRX Quantum* **5**, 020368 (2024).

[36] M. W. Sze, D. Z. Manrique, D. M. Ramo, and N. Fitzpatrick, Shorter width truncated Taylor series for Hamiltonian dynamics simulations (2025), [arXiv:2511.09461](https://arxiv.org/abs/2511.09461).

[37] I. Loaiza, A. M. Khah, N. Wiebe, and A. F. Izmaylov, Reducing molecular electronic Hamiltonian simulation cost for linear combination of unitaries approaches, *Quantum Sci. Technol.* **8**, 035019 (2023).

[38] R. H. Dicke, Coherence in spontaneous radiation processes, *Phys. Rev.* **93**, 99 (1954).

[39] A. Bartschi and S. Eidenbenz, Deterministic preparation of Dicke states, in *Fundamentals of Computation Theory* (Springer International Publishing, 2019) p. 126–139.

[40] A. Bartschi and S. Eidenbenz, Short-depth circuits for Dicke state preparation, in *2022 IEEE International Conference on Quantum Computing and Engineering (QCE)* (2022) pp. 87–96.

[41] L. Piroli, G. Styliaris, and J. I. Cirac, Approximating many-body quantum states with quantum circuits and measurements, *Phys. Rev. Lett.* **133**, 230401 (2024).

[42] J. Yu, S. R. Muleady, Y.-X. Wang, N. Schine, A. V. Gorshkov, and A. M. Childs, Efficient preparation of Dicke states (2024), [arXiv:2411.03428](https://arxiv.org/abs/2411.03428).

[43] R. C. Farrell, N. A. Zemlevskiy, M. Illa, and J. Preskill, Digital quantum simulations of scattering in quantum field theories using W states (2025), [arXiv:2505.03111](https://arxiv.org/abs/2505.03111).

[44] R. D. Somma, Quantum eigenvalue estimation via time series analysis, *New J. Phys.* **21**, 123025 (2019).

[45] S. Lu, M. C. Bañuls, and J. I. Cirac, Algorithms for quantum simulation at finite energies, *PRX Quantum* **2**, 020321 (2021).

[46] L. Lin and Y. Tong, Heisenberg-limited ground-state energy estimation for early fault-tolerant quantum computers, *PRX Quantum* **3**, 010318 (2022).

[47] N. S. Blunt, L. Caune, R. Izsák, E. T. Campbell, and N. Holzmann, Statistical phase estimation and error mitigation on a superconducting quantum processor, *PRX Quantum* **4**, 040341 (2023).

[48] A. Dutkiewicz, B. M. Terhal, and T. E. O’Brien, Heisenberg-limited quantum phase estimation of multiple eigenvalues with few control qubits, *Quantum* **6**, 830 (2022).

[49] B. F. Schiffer, D. S. Wild, N. Maskara, M. D. Lukin, and J. I. Cirac, Hardware-efficient quantum phase estimation via local control (2025), [arXiv:2506.18765](https://arxiv.org/abs/2506.18765).

[50] M. A. Nielsen and I. L. Chuang, *Quantum Computation and Quantum Information: 10th Anniversary Edition* (Cambridge University Press, 2011).

### Appendix A: Proof of Theorem 2

Applying the  $P_R(M_1)$  and  $P_R(M_2)$  oracles to the initial state  $|0\rangle_{2n}|0\rangle_{2n}|\varphi\rangle$  yields:

$$\begin{aligned} P_R(M_1)|0^{\otimes n}\rangle|0^{\otimes n}\rangle \otimes P_R(M_2)|0^{\otimes n}\rangle|0^{\otimes n}\rangle|\varphi\rangle \\ = \left( \sum_{i,j=0}^{2^n-1} e^{i(\arg(\alpha_{ij}))} \sqrt{|\alpha_{ij}|} |i\rangle|j\rangle \right) \otimes \left( \sum_{p,q=0}^{2^n-1} e^{i(\arg(\beta_{pq}))} \sqrt{|\beta_{pq}|} |p\rangle|q\rangle \right) |\varphi\rangle, \end{aligned} \quad (\text{A1})$$

where the tensor product can be expanded as:

$$\sum_{p,q,i,j=0}^{2^n-1} e^{i(\arg(\alpha_{ij})+\arg(\beta_{pq}))} \sqrt{|\alpha_{ij}\beta_{pq}|} |i\rangle|j\rangle|p\rangle|q\rangle|\varphi\rangle. \quad (\text{A2})$$

After the first  $n$  CNOTs and  $n$  CZs of the SELECT section, the state becomes:

$$\sum_{p,q,i,j=0}^{2^n-1} e^{i(\arg(\alpha_{ij})+\arg(\beta_{pq}))} \sqrt{|\alpha_{ij}\beta_{pq}|} |i\rangle|j\rangle|p\rangle|q\rangle \otimes \left( \bigotimes_{\ell=0}^{n-1} Z^{i_\ell} X^{j_\ell} \right) |\varphi\rangle, \quad (\text{A3})$$

and subsequently, after the other  $n$  CNOTs and  $n$  CZs, we get:

$$\sum_{p,q,i,j=0}^{2^n-1} e^{i(\arg(\alpha_{ij})+\arg(\beta_{pq}))} \sqrt{|\alpha_{ij}\beta_{pq}|} |i\rangle|j\rangle|p\rangle|q\rangle \otimes \left( \bigotimes_{\ell=0}^{n-1} Z^{q_\ell} X^{p_\ell} Z^{j_\ell} X^{i_\ell} \right) |\varphi\rangle. \quad (\text{A4})$$

Finally, we apply the left state preparation oracles  $P_L(M_1)^\dagger$  and  $P_L(M_2)^\dagger$  and we project onto the ancilla qubits:

$${}_{4n}\langle 0| P_L(M_2)^\dagger \otimes P_L(M_1)^\dagger = \sum_{p,q,i,j=0}^{2^n-1} \sqrt{|\alpha_{ij}\beta_{pq}|} \langle i| \langle j| \langle p| \langle q|, \quad (\text{A5})$$

so that we get the final (non-normalized) state:

$$\sum_{i,j,p,q=0}^{2^n-1} \alpha_{ij}\beta_{pq} \left( \bigotimes_{\ell=0}^{n-1} Z^{q_\ell} X^{p_\ell} Z^{j_\ell} X^{i_\ell} \right) |\varphi\rangle = C |\varphi\rangle, \quad (\text{A6})$$

for  $C$  defined in Eq. (37), which completes the proof.

### Appendix B: Proof of Theorem 3

We prove that the circuit in Fig. 1a correctly implements the matrix polynomial defined in Eq. (43). We begin by analyzing the action of  $POLY_R$ , defined in Eq. (54), on the initial state  $|0\rangle_d|0\rangle_{(2d+1)n}|\varphi\rangle$ . Applying  $POLY_R$  yields

$$|0\rangle_d|0\rangle_{(2d+1)n}|\varphi\rangle \xrightarrow{POLY_R} \frac{1}{\sqrt{\mathcal{W}}} \sum_{k=0}^d e^{i \sum_{j=0}^{k-1} \phi_j} \sqrt{|a_k| \mathcal{N}^k} |k_u\rangle|0\rangle_{2dn}|\varphi\rangle. \quad (\text{B1})$$

By definition of the unary-encoded states  $|k_u\rangle$  in Eq. (50), each such state contains exactly  $k$  leading ones. Consequently,  $|k_u\rangle$  activates precisely the first  $k$   $P_R$  gates in the circuit. Applying Corollary 4 to the normalized matrix  $\frac{\mathcal{H}}{\mathcal{N}}$ , we conclude that, after applying all  $P_R$ , SELECT, and  $P_L^\dagger$  oracles, followed by post-selection on the all-zero outcome of the  $2dn$  ancilla qubits on which  $P_R$  and  $P_L^\dagger$  act, the resulting state is:

$$\frac{1}{\mathcal{W}} \sum_{k=0}^d e^{i \sum_{j=0}^{k-1} \phi_j} \sqrt{|a_k| \mathcal{N}^k} |k_u\rangle \frac{\mathcal{H}^k}{\mathcal{N}^k} |\varphi\rangle. \quad (\text{B2})$$

Next, by applying  $\text{POLY}_L^\dagger$ , defined by Eq. (55), as well as measuring and post-selecting  $|0\rangle$  on the remaining  $d$  ancilla qubits, we obtain the (non-normalized) state:

$$\sum_{k=0}^d e^{i \sum_{j=0}^{k-1} \phi_j} |a_k| \mathcal{H}^k |\varphi\rangle. \quad (\text{B3})$$

Now, we just have to observe that from Eq. (45) we have:

$$\sum_{j=0}^{k-1} \phi_j = \arg(a_k) - \arg(a_0), \quad (\text{B4})$$

so that the final state in Eq. (B3) becomes:

$$e^{-i \arg(a_0)} \sum_{k=0}^d e^{i \arg(a_k)} |a_k| \mathcal{H}^k |\varphi\rangle = e^{-i \arg(a_0)} p_d(\mathcal{H}) |\varphi\rangle. \quad (\text{B5})$$

The resulting transformation is exactly the desired one, up to an irrelevant global phase  $e^{-i \arg(a_0)}$ , which completes the proof.

### Appendix C: $P_R$ circuits and resource estimation

In this section, we present an explicit construction of the  $P_R$  circuit for three one-dimensional spin models: the Heisenberg XYZ, Heisenberg XXZ, and Ising models. By explicitly leveraging the structure of the underlying Hamiltonians, we obtain implementations that are significantly more efficient than generic constructions.

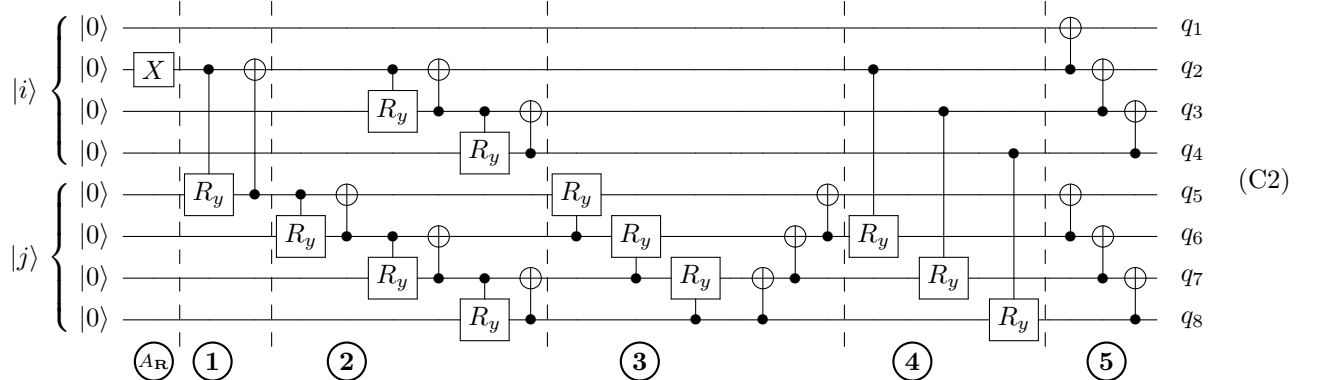
For each case, we provide the non-asymptotic resource analysis for both the FOQCS-LCU block encoding and the associated matrix-polynomial circuits, considering implementations with and without the additional overhead induced by controlling the entire circuit. Furthermore, we analyze two distinct assumptions on the connectivity of the physical device, namely all-to-all connectivity and a square-grid architecture.

#### 1. $P_R$ circuit and resource estimation for the one-dimensional Heisenberg XYZ model

We consider the one-dimensional XYZ Heisenberg model:

$$\mathcal{H} = g \sum_{i=0}^{n-1} Z_i + \sum_{i=0}^{n-2} J_x X_i X_{i+1} + J_y Y_i Y_{i+1} + J_z Z_i Z_{i+1}. \quad (\text{C1})$$

Figure 2 shows the circuit implementing the  $P_R$  oracle for such a model and for  $n = 4$ . For completeness, we repeat the circuit, and describe how to generalize it for other values of  $n$ .



For clarity, we denote the  $X$  and  $Z$  registers with the states  $|i\rangle$  and  $|j\rangle$  and we partition the  $P_R$  circuit into 6 sections, in which we specify the angles  $\theta$  required for the  $R_y$  gates.

$\textcircled{A_R}$ . The first gate acts as an *activation* for the whole circuit: the rest of the circuit has the state  $|0\rangle_{2n}$  as eigenstate, therefore, and following the notation from Assumption 1, the gate  $A_R$  corresponds to an  $X$  gate.

$\textcircled{1}$ . This gate corresponds to the gate  $\Gamma(\theta)$  defined in [27]. There, it was proven that it can be implemented with CNOT count and depth of 2. We define the standard angle as:

$$\tilde{\theta} = 2 \arccos \left( \sqrt{\frac{(|J_x| + |J_y|)(n-1)}{\mathcal{N}}} \right), \quad (\text{C3})$$

Then, the rotation angle depends on the sign of the coefficients  $g$  and  $J_x$ :

$$\theta = \begin{cases} \tilde{\theta}, & g \geq 0, J_x \geq 0, \\ 2\pi - \tilde{\theta}, & g \geq 0, J_x < 0, \\ \tilde{\theta} + 2\pi, & g < 0, J_x < 0, \\ -\tilde{\theta}, & g < 0, J_x \geq 0. \end{cases} \quad (\text{C4})$$

We remark that, even when adding angles of  $2\pi$ , the cosine and sine change because in the  $R_y$  gate, the cosine and sine are evaluated at  $\frac{\theta}{2}$ , as defined in Eq. (53).

$\textcircled{2}$ . Implementation of two balanced Dicke states [27, 39]:  $n-2$   $\Gamma$  gates on the  $X$  register and  $n-1$   $\Gamma$  gates on the  $Z$  register. The first rotation angle on the  $Z$  register is:

$$\theta_0 = 2 \arccos \left( \sqrt{\frac{|g|}{|g|n + |J_z|(n-1)}} \right), \quad (\text{C5})$$

while the other angles for both registers are defined as:

$$\theta_i = 2 \arccos \left( \sqrt{\frac{1}{n-i}} \right), \quad (\text{C6})$$

for  $i = 1, \dots, n-2$ . The total CNOT count is  $2(2n-3)$  since we have  $2n-3$   $\Gamma$  gates.

$\textcircled{3}$ . Acting on the  $Z$  register, we have a ladder of  $n-1$  controlled  $R_y$  gates with constant angles:

$$\theta = \begin{cases} \tilde{\theta} & g \cdot J_z \geq 0 \\ -\tilde{\theta} & g \cdot J_z < 0 \end{cases}, \quad \tilde{\theta} = 2 \arccos \left( \sqrt{\frac{|g|}{|g| + |J_z|}} \right). \quad (\text{C7})$$

Then we apply a ladder of  $n-1$  CNOT gates. The total CNOT count of this part is  $3(n-1)$  since we need 2 CNOTs to decompose each controlled  $R_y$  gate.

$\textcircled{4}$ . Ladder of  $n-1$   $R_y$  gates connecting the two registers, with constant rotation angles:

$$\theta = \begin{cases} \tilde{\theta} & J_x \cdot J_y \leq 0 \\ -\tilde{\theta} & J_x \cdot J_y > 0 \end{cases}, \quad \tilde{\theta} = 2 \arccos \left( \sqrt{\frac{|J_x|}{|J_x| + |J_y|}} \right). \quad (\text{C8})$$

This part needs  $2(n-1)$  CNOTs.

$\textcircled{5}$ . A ladder of  $n-1$  CNOTs is finally added on both registers.

For  $P_L$ , the structure of the circuit is the same as Eq. (C2). Since the phase information of the Hamiltonian coefficients is entirely stored in  $P_R$ , we choose the standard rotation angles  $\theta \equiv \tilde{\theta}$  throughout the  $P_L$  circuit.

The resource analysis for the state preparation oracles, the entire FOQCS-LCU block encoding and the matrix polynomial algorithm presented in Section IV B is reported in Table I. We consider both the all-to-all connectivity and the square grid connectivity.

Circuit	CNOT count		CNOT depth		Number of qubits	
	all-to-all	square grid	all-to-all	square grid	all-to-all	square grid
P <sub>R</sub> /P <sub>L</sub> Controlled-P <sub>R</sub> /P <sub>L</sub>	8n - 8	8n - 8	2n + 6	2n + 6	2n	2n
	8n - 7	8n - 7	2n + 7	2n + 7	2n + 1	2n + 1
FOQCS-LCU Controlled-FOQCS-LCU	18n - 16	20n - 16	4n + 14	4n + 16	3n	3n
	18n - 14	20n - 14	4n + 16	4n + 18	3n + 1	3n + 1
p <sub>d</sub> (H) Controlled-p <sub>d</sub> (H)	18dn - 12d - 4	20dn - 4d - 6	4n + 6d + 10	4n + 10d + 12	2dn + d + n	2dn + 2d + n
	18dn - 12d	20dn - 4d - 2	4n + 6d + 14	4n + 10d + 16	2dn + d + n + 1	2dn + 2d + n + 1

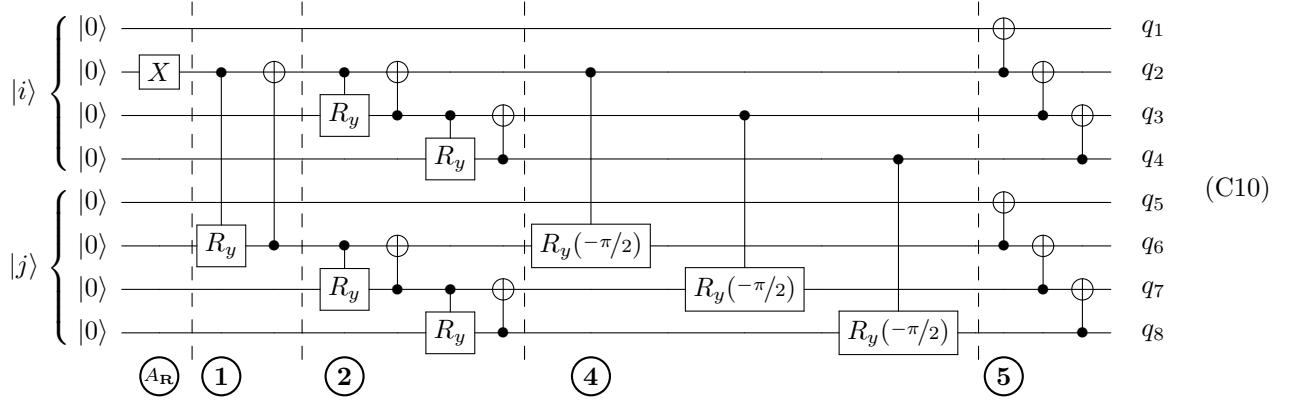
Table II: Resource analysis for the P<sub>R</sub> and P<sub>L</sub><sup>†</sup> oracles, the FOQCS-LCU block encoding, a generic matrix polynomial of H and their controlled circuits for the one-dimensional XXZ Heisenberg Hamiltonian defined in Eq. (C9).

## 2. P<sub>R</sub> circuit and resource estimation for the one-dimensional Heisenberg XXZ model

Next, we show how the circuit in Fig. 2 (and equivalently Eq. (C2)), further simplifies when we have  $g = 0$  and  $J_x = J_y = J$ , i.e, the XXZ model:

$$\mathcal{H} = \sum_{i=0}^{n-2} J X_i X_{i+1} + J Y_i Y_{i+1} + J_z Z_i Z_{i+1}. \quad (\text{C9})$$

More specifically, the circuit for P<sub>R</sub> is:



Following the same structure as in Section C1, we only list and describe the sections in Eq. (C10) that differ from Eq. (C2):

- ①. Same as Eq. (C2), except the target of  $R_y$  and the control of the following CNOT is on the second qubit of the Z register instead of the first.
- ②. Implementation of two balanced Dicke states [27, 39]:  $n - 2$   $\Gamma$  gates on both the X and Z register, with rotation angles as defined in Eq. (C6).
- ③. There is no equivalent section here compared to Eq. (C2).
- ④. Ladder of  $n - 1$   $R_y$  gates connecting the two registers. Since  $J_x = J_y$ , Eq. (C8) becomes:

$$\theta = -\tilde{\theta} = -\frac{\pi}{2}. \quad (\text{C11})$$

For P<sub>L</sub>, the structure of the circuit is the same as Eq. (C10). Since the phase information of the Hamiltonian coefficients is entirely stored in P<sub>R</sub>, we choose the standard rotation angles  $\theta \equiv \tilde{\theta}$  throughout the P<sub>L</sub> circuit. For instance, Eq. (C11) becomes  $\theta = \pi/2$ . A resource analysis of the presented circuits for the one-dimensional Heisenberg XXZ model is summarized in Table II.

Circuit	CNOT count		CNOT depth		Number of qubits	
	all-to-all	square grid	all-to-all	square grid	all-to-all	square grid
P <sub>R</sub> /P <sub>L</sub> Controlled-P <sub>R</sub> /P <sub>L</sub>	5n - 5	5n - 1	2n	2n + 4	2n	2n
	5n - 4	5n	2n + 1	2n + 5	2n + 1	2n + 1
FOQCS-LCU Controlled-FOQCS-LCU	12n - 10	14n - 2	4n + 2	4n + 10	3n	3n
	12n - 8	14n	4n + 4	4n + 12	3n + 1	3n + 1
p <sub>d</sub> (H) Controlled-p <sub>d</sub> (H)	12dn - 6d - 4	14dn + 11d - 6	4n + 6d - 2	4n + 10d + 8	2dn + d + n	2dn + 2d + n
	12dn - 6d	14dn + 11d - 2	4n + 6d + 2	4n + 10d + 12	2dn + d + n + 1	2dn + 2d + n + 1

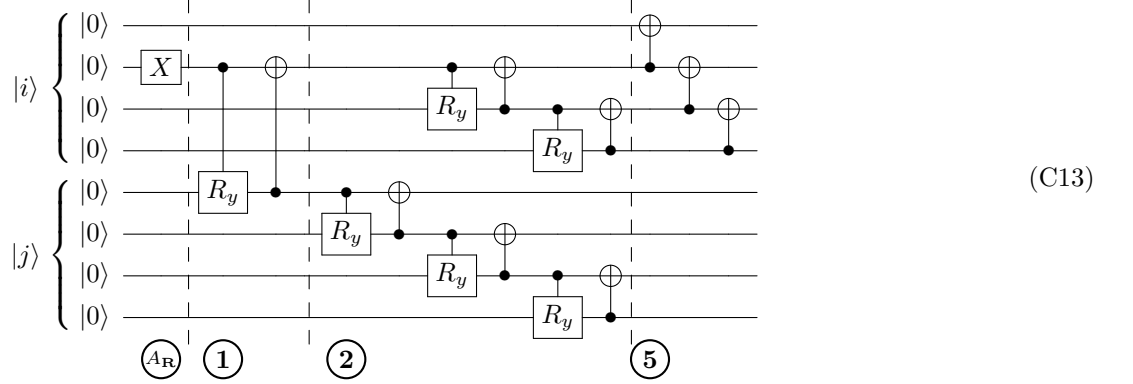
Table III: Resource analysis for the P<sub>R</sub> and P<sub>L</sub><sup>†</sup> oracles, the FOQCS-LCU block encoding, a generic matrix polynomial of H and their controlled circuits for the one-dimensional Ising Hamiltonian defined in Eq. (C12).

### 3. P<sub>R</sub> circuit and resource estimation for the one-dimensional Ising model

Finally, we focus on how to simplify the circuit implementing the P<sub>R</sub> oracles presented in the previous sections, for the Ising model, where the Hamiltonian is defined as:

$$\mathcal{H} = g \sum_{i=0}^{n-1} Z_i + J \sum_{i=0}^{n-2} X_i X_{i+1}. \quad (\text{C12})$$

The circuit for P<sub>R</sub> is the following:



Looking at the P<sub>R</sub> circuit defined in Eq. (C2) for the XYZ Heisenberg model, we notice that the sections ④<sub>R</sub>, ①, and ② are identical, while the sections ③ and ④ are missing. The only section that differs is ⑤, where instead of having one CNOT ladder on both the first and second ancilla registers, we only have one ladder in the first register.

For P<sub>L</sub>, the structure of the circuit is the same as Eq. (C13). Since the phase information of the Hamiltonian coefficients is entirely stored in P<sub>R</sub>, we choose the standard rotation angles  $\theta \equiv \tilde{\theta}$  throughout the P<sub>L</sub> circuit. A resource analysis of the circuits presented in this paper for the specific case of the Ising model is presented in Table III.

### Appendix D: Explicit 2D circuits with square grid connectivity

Standard quantum circuits are typically described using a one-dimensional (1D) qubit ordering and assume arbitrary two-qubit interactions. In contrast, real quantum hardware often restricts two-qubit gates to nearest-neighbor interactions on a two-dimensional (2D) square grid. In this section, we describe how to map 1D circuits onto a 2D qubit layout that respects these qubit connectivity constraints.

We present explicit 2D circuit implementations for the SELECT oracle of the FOQCS-LCU block encoding and for the P<sub>R</sub> oracle in the specific case of the one-dimensional XXZ Heisenberg model. Assuming square-grid connectivity, we begin by mapping the qubits of the original 1D circuit onto the 2D grid.

The FOQCS-LCU block encoding consists of three qubit registers: n qubits for the X register, denoted by |i>, n qubits for the Z register, denoted by |j>, and n qubits for the input quantum state |φ>. We therefore arrange these qubits in a rectangular 3 × n layout, as shown in Fig. 6 for the case n = 6.

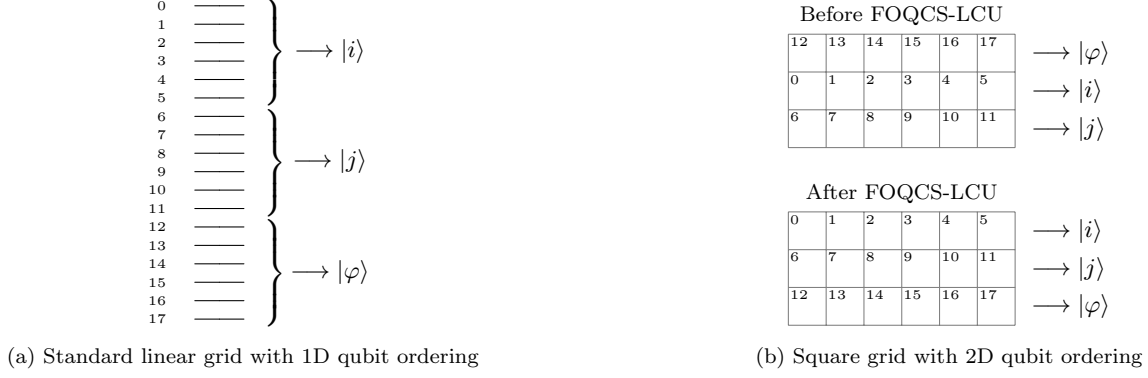


Figure 6: Qubit ordering for (a) 1D layout and (b) 2D layout of the quantum circuit implementing the FOQCS-LCU block encoding, assuming square grid connectivity. The grid consists of  $3 \times n$  qubits, here visualized for  $n = 6$ .  $|\varphi\rangle$ ,  $|i\rangle$  and  $|j\rangle$  correspond to the system,  $X$ , and  $Z$  registers, respectively.

### 1. 2D circuits of the SELECT oracle

Starting from the qubit mapping in Fig. 6, we now discuss how to implement the SELECT oracle of the FOQCS-LCU block encoding.

First, we notice that while the  $X$  register and the system qubits are directly connected, we need to perform SWAP gates to bring the  $Z$  register and the system qubits close to each other. The 2D circuit is shown in Fig. 7. We remark that each SWAP gate can be decomposed into three CNOTs [50]. Since  $n$  CNOTs are applied immediately after the first  $n$  SWAP gates on the same qubits, these operations can be merged, yielding in a total of  $2n$  CNOTs for the first two diagrams of Fig. 7. Similarly, the CZ gates and the final layer of SWAPs can also be merged:

$$\begin{array}{c} \bullet \quad \times \\ \bullet \quad \times \end{array} = \begin{array}{c} \boxed{H} \quad \oplus \quad \boxed{H} \quad \times \\ \bullet \quad \bullet \quad \bullet \quad \bullet \quad \bullet \quad \bullet \end{array} = \begin{array}{c} \boxed{H} \quad \oplus \quad \times \\ \bullet \quad \bullet \quad \bullet \quad \bullet \quad \bullet \quad \bullet \end{array} \boxed{H} = \begin{array}{c} \boxed{H} \quad \bullet \quad \oplus \\ \bullet \quad \bullet \quad \bullet \quad \bullet \quad \bullet \quad \bullet \end{array} \boxed{H} \quad (D1)$$

Note that this simplification is made possible by the choice of inverting the system register  $|\varphi\rangle$  with the ancilla registers  $|i\rangle$  and  $|j\rangle$  after the SELECT operation. Overall, the construction requires  $4n$  CNOTs and has a CNOT depth equal to 4.

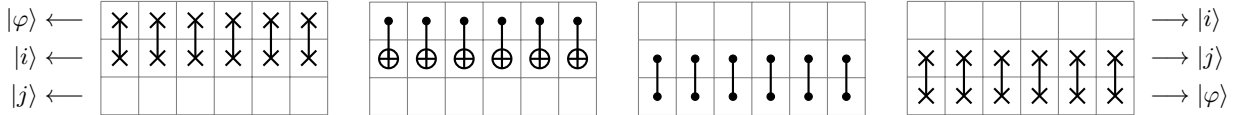


Figure 7: 2D quantum circuit implementing the SELECT oracle for  $n = 6$  and assuming grid connectivity.

### 2. 2D circuits of the $P_R$ oracle

In this section, we utilize the 2D qubit mapping from Fig. 6 to implement the  $P_R$  oracle of the FOQCS-LCU block encoding on a quantum device with 2D grid connectivity. Since the state preparation oracles differ between models, here we consider the specific case of the one-dimensional XXZ Heisenberg model defined in Section C2. The results can be immediately generalized to the other spin Hamiltonians presented in this paper.

Starting from the  $P_R$  circuit from Eq. (C10), the two-dimensional circuit is shown in Fig. 8 for the case  $n = 6$ .  $P_L$  follows the same construction and just differs in the rotation angles, as explained in Section C2.

### 3. 2D circuit description for the matrix polynomial block encoding

Finally, we show the 2D qubit mapping utilized for the circuits in Fig. 1. Starting from the layout in Fig. 6, the registers  $|i_k\rangle$  and  $|j_k\rangle$  for  $k = 0, \dots, d-1$  are stacked vertically, as shown in Fig. 9. In addition, a column of  $2d$

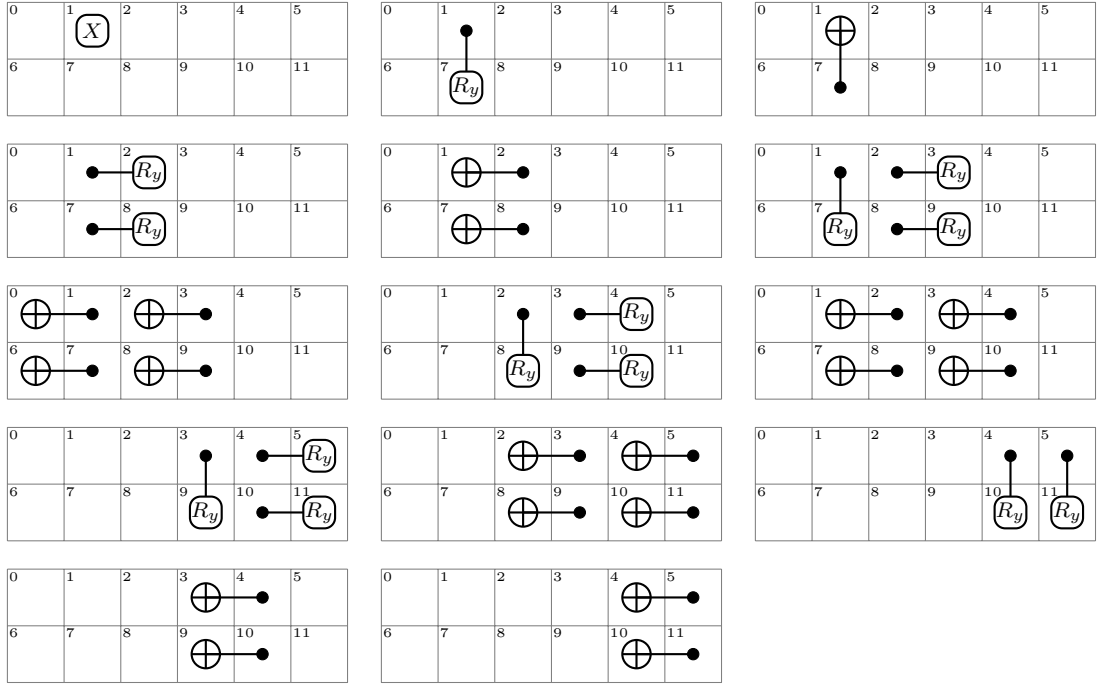
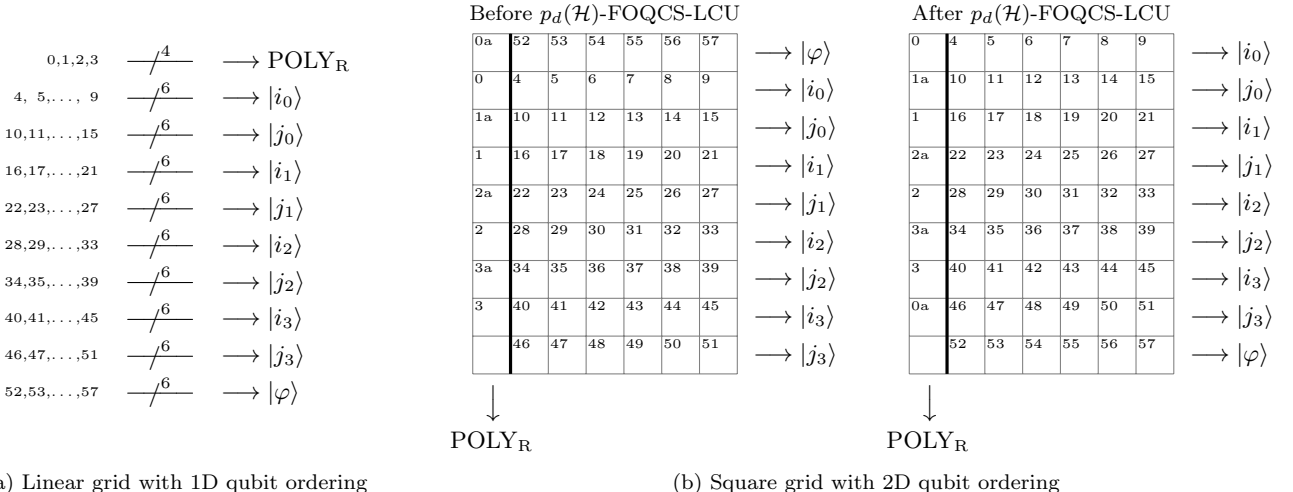


Figure 8: 2D quantum circuit implementing the  $P_R$  oracle of the one-dimensional XXZ Heisenberg model. We assume  $n = 6$  and square grid connectivity.

ancillary qubits is placed on the left-hand side of the layout.



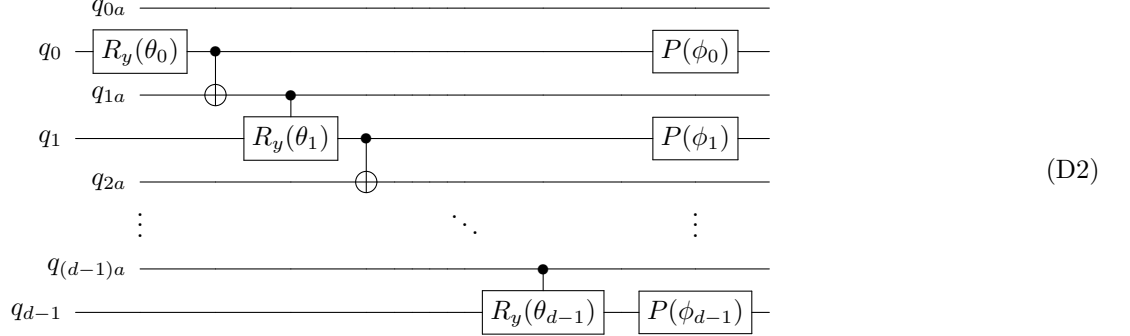
(a) Linear grid with 1D qubit ordering

(b) Square grid with 2D qubit ordering

Figure 9: Qubit ordering for (a) 1D layout and (b) 2D layout of the quantum circuit implementing the matrix polynomial encoding shown in Fig. 1. The grid consists of  $2d + (2d + 1)n$  qubits, here visualized for  $n = 6$  and  $d = 4$ . The first  $2d$  qubits are positioned in the first column to implement the  $POLY_R$  gate as described in Eq. (D2).

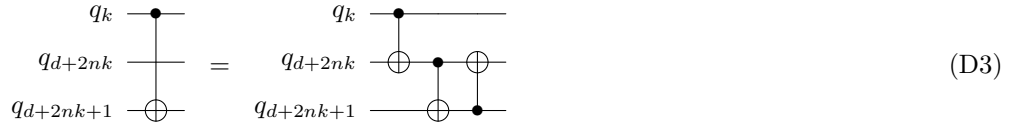
On these additional  $2d$  ancillary qubits, we implement modified versions of the  $POLY_R$  and  $POLY_L$  oracles, differing from their standard realizations presented in Lemmas 3 and 4. In particular, following the qubit mapping of Fig. 9,

we redefine the circuit implementing  $\text{POLY}_R$  as follows:



The rationale behind doubling the number of qubits used to implement  $\text{POLY}_R$  can be understood by inspecting Fig. 1b in the specific setting where  $P_R$  and  $P_L$  admit the decompositions given in Eqs. (60) and (61). After applying  $\text{POLY}_R$ , one encounters  $d$  CNOT gates with target on the second qubit of each  $|i_k\rangle$  ancilla register. Consequently, it is advantageous for the  $d$  controlling qubits, on which  $\text{POLY}_R$  acts, to be placed as close as possible to the corresponding target qubits in the  $|i_k\rangle$  registers. This proximity is achieved by interleaving these  $d$  qubits with an additional set of  $d-1$  qubits, using the modified implementation shown in Eq. (D2). We remark that the wire  $q_{0a}$  is intentionally left unused in  $\text{POLY}_R$ ; however, it is needed for  $\text{POLY}_L$ , as described below.

Even with this layout, for  $k = 0, \dots, d-1$ , the control qubit  $q_k$  and its corresponding target qubit in the  $|i_k\rangle$  register, namely  $q_{d+2nk+1}$ , are still not nearest neighbors. A CNOT gate between these two qubits can be implemented using three nearest-neighbor CNOT gates:



With these explicit circuits for  $\text{POLY}_R$  and for the CNOT gates activating each block-encoding of  $\mathcal{H}$ , the full 2D circuit for encoding a polynomial proceeds as follows:

1. Apply  $\text{POLY}_R$  on qubits  $q_{0a}$  through  $q_d$  (leftmost column in Fig. 9) following Eq. (D2).
2. Apply the “distance-2 CNOT” gate, Eq. (D3), on each pair  $q_k, q_{d+2nk+1}$ , for controlled activation of each  $P_R$ .
3. Apply  $\tilde{P}_R$  on each pair of ancilla registers:  $(i_0, j_0), \dots, (i_{d-1}, j_{d-1})$ .
4. Successively apply  $d$  SELECT oracles, Fig. 7, from top to bottom. First we apply it on registers  $(\varphi, i_0, j_0)$ , and in the process the  $\varphi$  register is swapped with the ancillae, so that the order from top to bottom reads  $i_0, j_0, \varphi, i_1, \dots$ . Then repeat on  $(\varphi, i_1, j_1)$ , after which the data register  $\varphi$  ends up below  $j_1$ . Continuing in this fashion, after  $d$  applications we now have the data register in the lowest row, and all ancilla registers shifted up by 1.
5. In parallel with the previous step, we also apply SWAPs to move all the ancillae in the leftmost column, used for  $\text{POLY}_R$  and  $\text{POLY}_L$  up by 1.
6. Apply  $\tilde{P}_L^\dagger$  on each pair of ancilla registers (now shifted up by 1 row relative to where we applied  $\tilde{P}_R$ ).
7. Apply the  $d$  “distance-2 CNOT” gates, Eq. (D3), but shifted up by one row relative to where they were previously applied.
8. Apply  $\text{POLY}_L^\dagger$  in analogous form to Eq. (D2), but with all gates shifted up by one qubit in the 2D layout.  $q_{0a}$  is still unused, but is in a different physical location.
9. Measure all ancilla registers  $i_0, \dots, j_{d-1}$  and the  $2d$  qubits of the leftmost column and post-select on outcome  $|0\rangle$  on each, then the output state with the polynomial applied is stored in the  $\varphi$  register, now at the bottom row of the grid.

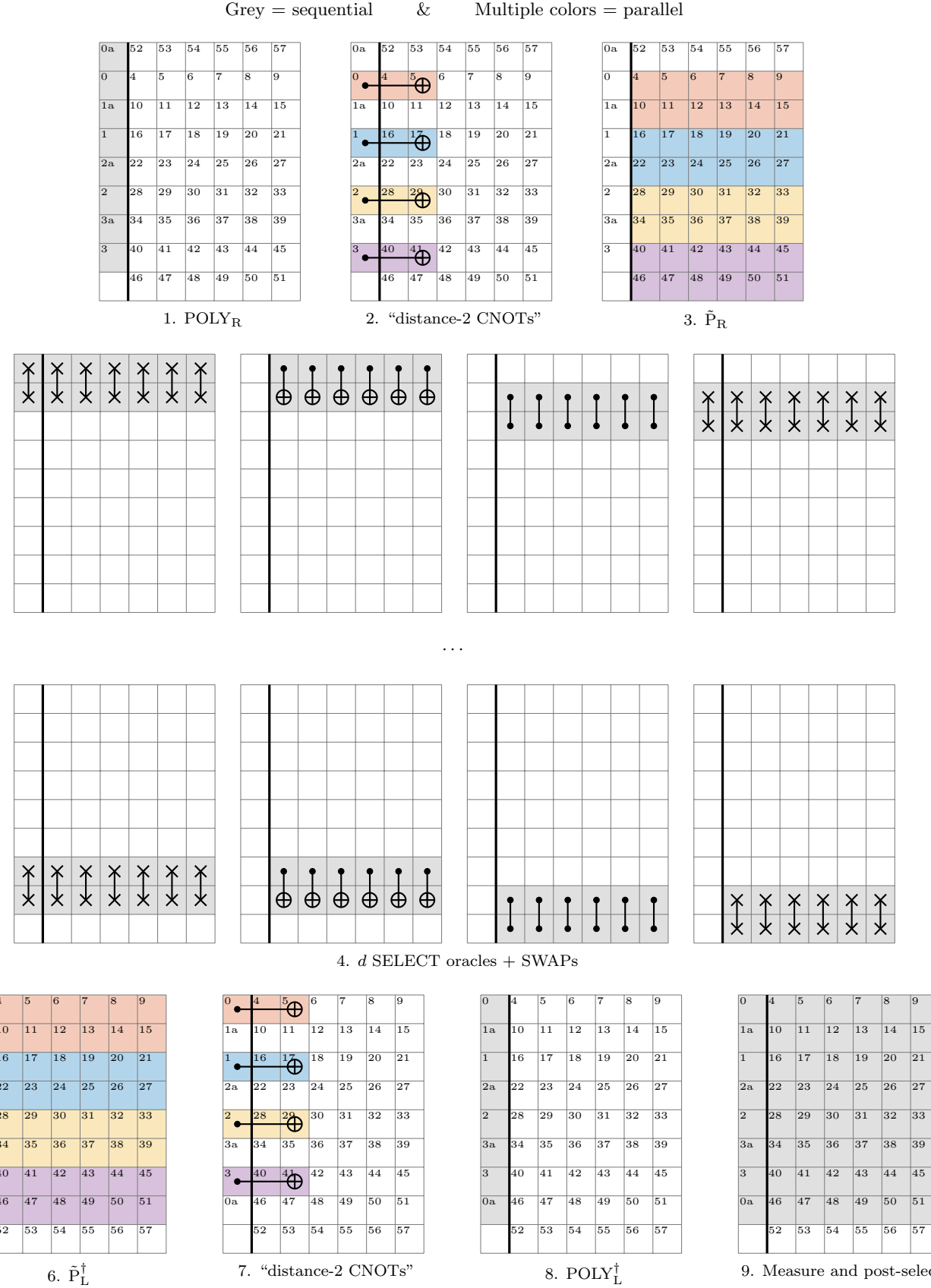


Figure 10: 2D circuit mapping for the matrix polynomial transformation algorithm based on FOQCS-LCU for  $n = 6$  and  $d = 4$ . The one-dimensional version is shown in Fig. 1b, where  $A_R$  and  $A_L$  reduce to a single  $X$  gate on the second qubit of each  $|i_k\rangle$  register.

**Appendix E: Matrix polynomial full circuit for the Ising Hamiltonian for  $n = 3$  and  $d = 3$**

